

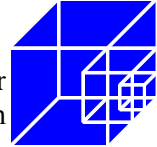
# Stainless Steel in Fire

WP 1 Fire Resistant Structures and Products

**WP 1.5. Numerical Studies**

**Final report**

<b>Contractor:</b>	Institute for Steel Construction Leibniz University Hannover (LUH) Appelstrasse 9a 30167 Hannover Germany
<b>Contact Person:</b>	Prof. Dr.-Ing. Peter Schaumann
<b>Scientific Staff:</b>	Dipl.-Ing. Oliver Bahr Dr.-Ing. Alexander Heise Dipl.-Ing. Florian Kettner
<b>Funding:</b>	Research Program of the Research Fund for Coal and Steel
<b>Pages:</b>	55
<b>Date:</b>	29 March 2007



## **1 Executive Summary**

The aim of this work package is to develop new stainless steel products without fire protection that achieve fire resistance classifications R30 or R60. The new products will include fire-separating members and load-bearing structures.

To identify reasonable field of application for stainless steel, material properties at elevated temperatures are compared to those of carbon steel at first.

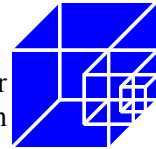
Numerical investigations on a new stainless steel slab panel with rock wool insulation follow as a typical example for fire-separating members. Results of the calculation at elevated temperatures demonstrate that a required fire resistance time of 60 minutes can be achieved.

Moreover, numerical studies on different load-bearing structures are performed. It is proved that it is possible to meet fire safety requirements for 30 or 60 minutes with unprotected or partially protected stainless steel load-bearing structures.



## **2 Contents**

<b>1</b>	<b>Executive Summary</b>	<b>2</b>
<b>2</b>	<b>Contents</b>	<b>3</b>
<b>3</b>	<b>Introduction</b>	<b>4</b>
<b>4</b>	<b>Objectives</b>	<b>4</b>
<b>5</b>	<b>Numerical Analysis</b>	<b>5</b>
5.1	Software	5
5.2	Material modelling	5
5.2.1	Mechanical Properties at ambient temperature	5
5.2.2	Mechanical properties at elevated temperatures	5
5.2.3	Thermal properties	10
5.3	Separating members	13
5.3.1	Task and introduction	13
5.3.2	Geometry of the test specimen	13
5.3.3	Material properties	14
5.3.4	Fire tests	14
5.3.5	Finite Element Models	16
5.3.6	Procedure at elevated temperatures	18
5.3.7	Results	21
5.4	Load-bearing structures	31
5.4.1	Nested tubes	31
5.4.2	Column in SIPOREX wall	41
<b>6</b>	<b>Development of design guidance</b>	<b>53</b>
<b>7</b>	<b>Conclusions</b>	<b>54</b>
7.1	Separating structures	54
7.2	Load-bearing structures	54
<b>8</b>	<b>Recommendations for further work</b>	<b>54</b>
<b>9</b>	<b>References</b>	<b>55</b>



### 3 Introduction

Stainless steel is characterised by numerous advantages, such as high corrosion resistance, durability, ease of maintenance and in particular aesthetics. So far, this construction material is mainly chosen for these reasons. The main disadvantage is the difference between prices of stainless and carbon steel. As a rule of thumb, the initial costs for stainless steel are four to five times higher than that of carbon steel. Although stainless steel becomes economically more attractive when considering its low life-cycle costs, it is often not the first choice as structural element.

However, existing data on the structural behaviour of stainless steel exposed to fire indicates additional benefits. In comparison to carbon steel, austenitic grades of stainless steel retain higher strengths for temperature above 500°C and higher modulus of elasticity for temperatures above 200°C. This superior material behaviour at elevated temperatures may help to justify the use of stainless instead of carbon steel.

In this work package, material properties of stainless steel were compared to those of carbon steel. The comparison included thermal as well as mechanical material properties, which were implemented in established numerical models.

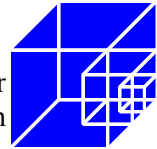
Numerical studies began with a new type of laser-welded stainless steel slab panel with rock wool insulation, which has been developed by Kenno Tech Ltd.. Apart from the general load-bearing behaviour at ambient and elevated temperatures, it was examined if this separating structure is able to fulfil the insulation criterion of EN 1993-1-2 for separating members.

Different load-bearing structures were examined subsequently in order to meet requirements for 30 and 60 minutes fire resistance. So-called nested tubes were initially investigated, where the cross-section consists out of tubes within each other and the space between the profiles is insulated with mineral wool. In addition, an unprotected stainless steel column was regarded. Numerical studies close with the examination on the load-bearing behaviour of a stainless steel column integrated in a SIPOREX wall.

On basis of previous investigations, design guidance was given and conclusions for the reasonable use of stainless steel in separating members and load-bearing structures were drawn.

### 4 Objectives

There is a high difference between prices of carbon and stainless steel. Therefore this work package aims at the identification of structural solutions where stainless steel shows distinctive advantages over carbon steel. The main objective is to develop new stainless steel products without passive or active fire protection that can meet fire safety requirements for 30 or 60 minutes. The new products will include fire-separating members and load-bearing structures.



## **5 Numerical Analysis**

### **5.1 Software**

Two different software packages were used for numerical analyses. The Finite Element-code ABAQUS/Standard, version 6.6 and the transient, non-linear, incremental computer code BoFIRE. The latter finite element based program, which was written by Schaumann [4], is capable of predicting thermal and structural behaviour of both steel and composite frame structures exposed to fire.

### **5.2 Material modelling**

#### **5.2.1 Mechanical properties at ambient temperature**

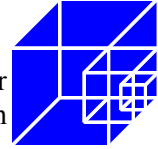
The material properties for stainless steel grade EN 1.4301 at room temperature were taken according to prEN 1993-1-4 [3] with following nominal values at room temperature:

- $f_y = 230 \text{ N/mm}^2$
- $f_u = 520 \text{ N/mm}^2$
- $E = 200,000 \text{ N/mm}^2$

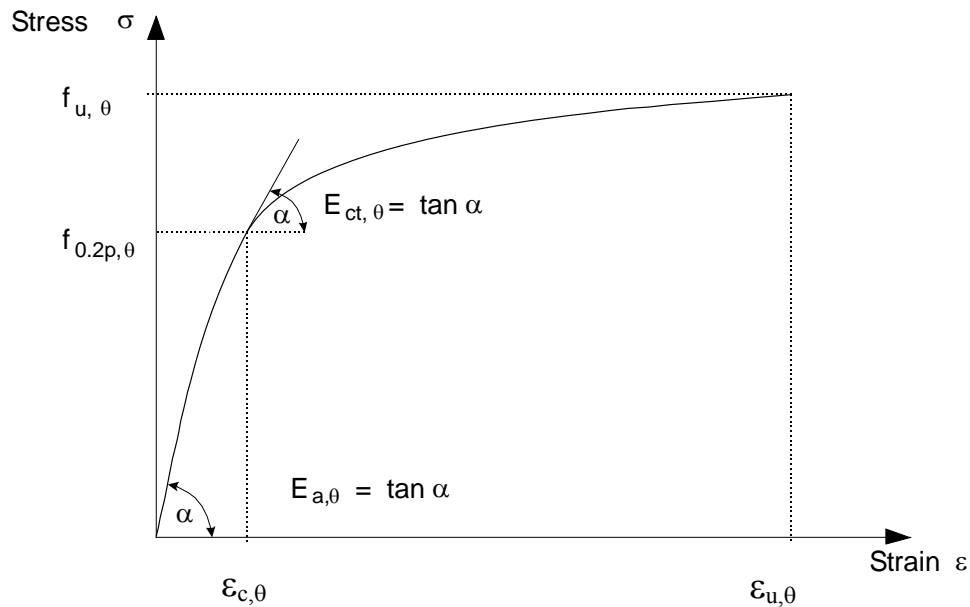
The unit mass of stainless steel is  $\rho = 7,900 \text{ kg/m}^3$ .

#### **5.2.2 Mechanical properties at elevated temperatures**

The stress-strain relationship for stainless steel at elevated temperatures was taken from EN 1993-1-2 [2]. The required formulas and tabulated data are demonstrated on the following pages.

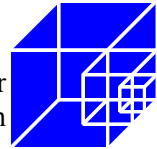


Strain range	Stress $\sigma$	Tangent modulus $E_t$
$\varepsilon \leq \varepsilon_{c,\theta}$	$\frac{E \times \varepsilon}{1 + a \times \varepsilon^b}$	$\frac{E(1 + a \times \varepsilon^b - a \times b \times \varepsilon^b)}{(1 + a \times \varepsilon^b)^2}$
$\varepsilon_{c,\theta} < \varepsilon \leq \varepsilon_{u,\theta}$	$f_{0.2p,\theta} - e + (d/c) \sqrt{c^2 - (\varepsilon_{u,\theta} - \varepsilon)^2}$	$\frac{d + (\varepsilon_{u,\theta} - \varepsilon)}{c \sqrt{c^2 - (\varepsilon_{u,\theta} - \varepsilon)^2}}$
Parameters	$\varepsilon_{c,\theta} = f_{0.2p,\theta} / E_{a,\theta} + 0.002$	
Functions	$a = \frac{E_{a,\theta} \varepsilon_{c,\theta} - f_{0.2p,\theta}}{f_{0.2p,\theta} \varepsilon_{c,\theta}^b} \quad b = \frac{(1 - \varepsilon_{c,\theta} E_{ct,\theta} / f_{0.2p,\theta}) E_{a,\theta} \varepsilon_{c,\theta}}{(E_{a,\theta} \varepsilon_{c,\theta} / f_{0.2p,\theta} - 1) f_{0.2p,\theta}}$ $c^2 = (\varepsilon_{u,\theta} - \varepsilon_{c,\theta}) \left( \varepsilon_{u,\theta} - \varepsilon_{c,\theta} + \frac{e}{E_{ct,\theta}} \right) \quad d^2 = e (\varepsilon_{u,\theta} - \varepsilon_{c,\theta}) E_{ct,\theta} + e^2$ $e = \frac{(f_{u,\theta} - f_{0.2p,\theta})^2}{(\varepsilon_{u,\theta} - \varepsilon_{c,\theta}) E_{ct,\theta} - 2(f_{u,\theta} - f_{0.2p,\theta})}$	

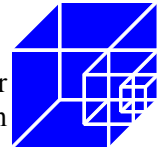


with

- $f_{u,\theta}$  tensile strength;
- $f_{0.2p,\theta}$  proof strength at 0.2% plastic strain;
- $E_{a,\theta}$  slope of the linear elastic range;
- $E_{ct,\theta}$  slope at proof strength;
- $\varepsilon_{c,\theta}$  total strain at proof strength;
- $\varepsilon_{u,\theta}$  ultimate strain.



Steel $\Theta_a$ <b>1.4301</b>	$k_{E,\theta} = E_{a,\theta}/E_a$	$k_{0.2p,\theta} = f_{0.2p,\theta}/f_y$	$k_{u,\theta} = f_{u,\theta}/f_u$	$f_{y,\theta}$ $k_{2\%,\theta}$
20	1.00	1.00	1.00	0.26
100	0.96	0.82	0.87	0.24
200	0.92	0.68	0.77	0.19
300	0.88	0.64	0.73	0.19
400	0.84	0.60	0.72	0.19
500	0.80	0.54	0.67	0.19
600	0.76	0.49	0.58	0.22
700	0.71	0.40	0.43	0.26
800	0.63	0.27	0.27	0.35
900	0.45	0.14	0.15	0.38
1,000	0.20	0.06	0.07	0.40
1,100	0.10	0.03	0.03	0.40
1,200	0.00	0.00	0.00	0.40



Steel $\Theta_a$ <b>1.4301</b>	$k_{\text{Ect},\theta} = E_{\text{ct},\theta}/E_a$	$\varepsilon_{u,\theta} [-]$
20	0.11	0.40
100	0.05	0.40
200	0.02	0.40
300	0.02	0.40
400	0.02	0.40
500	0.02	0.40
600	0.02	0.35
700	0.02	0.30
800	0.02	0.20
900	0.02	0.20
1000	0.02	0.20
1100	0.02	0.20
1200	0.02	0.20

For the numerical studies in ABAQUS true stresses and logarithmic strains were used.

$$\sigma_{\text{true}} = \sigma_{\text{nom}} (1 + \varepsilon_{\text{nom}}) \quad (1)$$

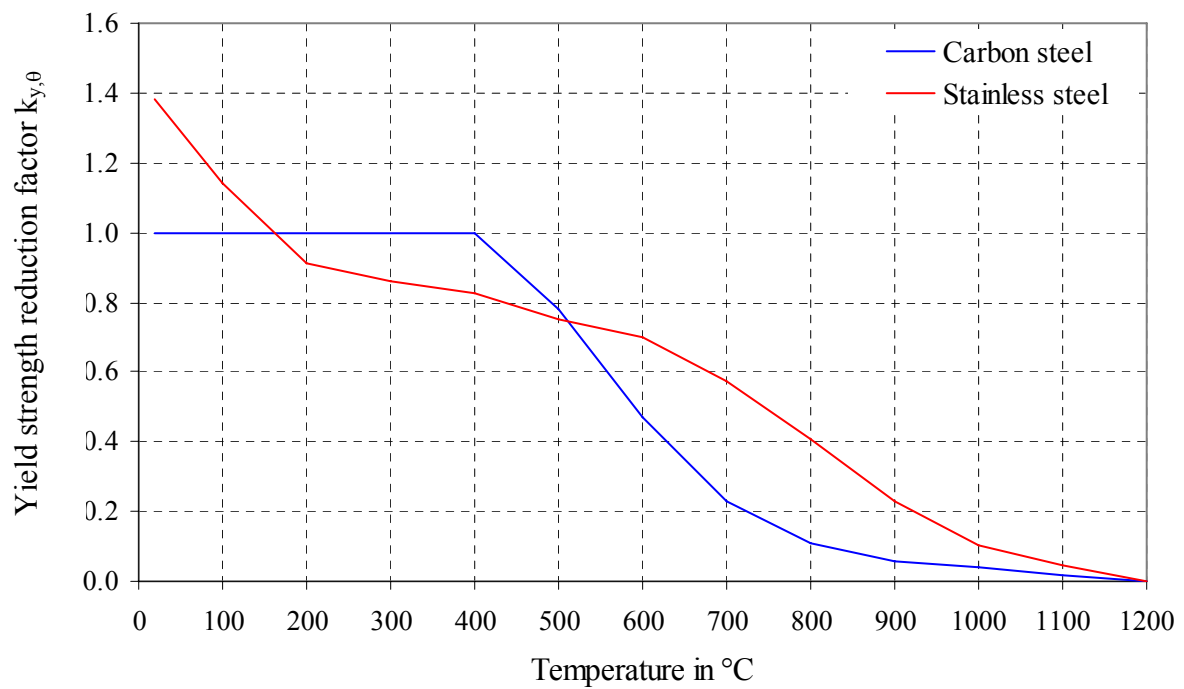
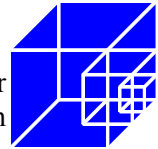
$$\varepsilon_{\text{ln}}^{\text{pl}} = \ln(1 + \varepsilon_{\text{nom}}) - \frac{\sigma_{\text{true}}}{E} \quad (2)$$

Figure 1 compares retention of strength for stainless and carbon steel at elevated temperatures. As a result of the beneficial effects of the alloying elements, stainless steel maintains its strength better than carbon steel at temperatures exceeding approximately 500°C.

Stainless steel shows even more distinctive advantages over carbon steel regarding stiffness retention at elevated temperatures. As it can be seen in Figure 2, stiffness of stainless steel specimens is reduced moderately in comparison to carbon steel, which is in particular true for temperatures up to 700°C. For higher temperatures degradation of strength is more severe.

The complete stress-strain relationship of both materials is presented in Figure 3 at the example of cross-sectional temperatures of 100°C, 300°C, 500°C and 700°C. In contrast to carbon steel, stainless steel is characterised by a rounded stress-strain curve with no sharp yield point and strain hardening. In addition, ultimate strains of stainless steel exceed those of carbon steel by far.





**Figure 1** Comparison of yield strength reduction at elevated temperatures

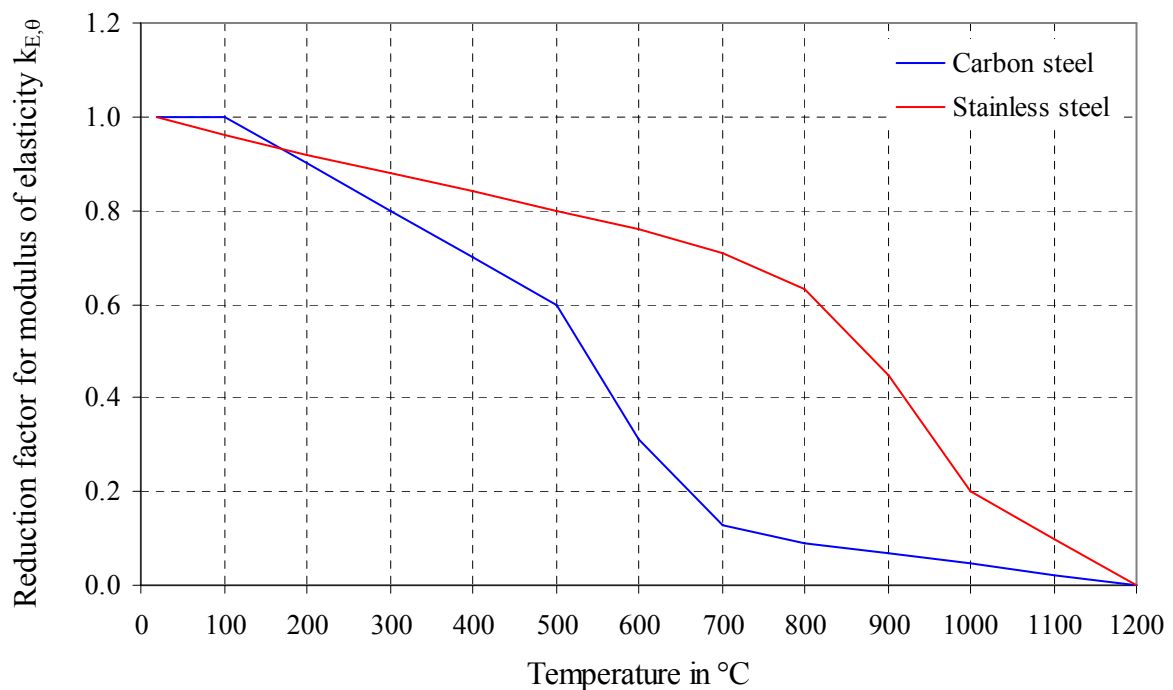


**Figure 2** Comparison of reduction of modulus of elasticity at elevated temperatures

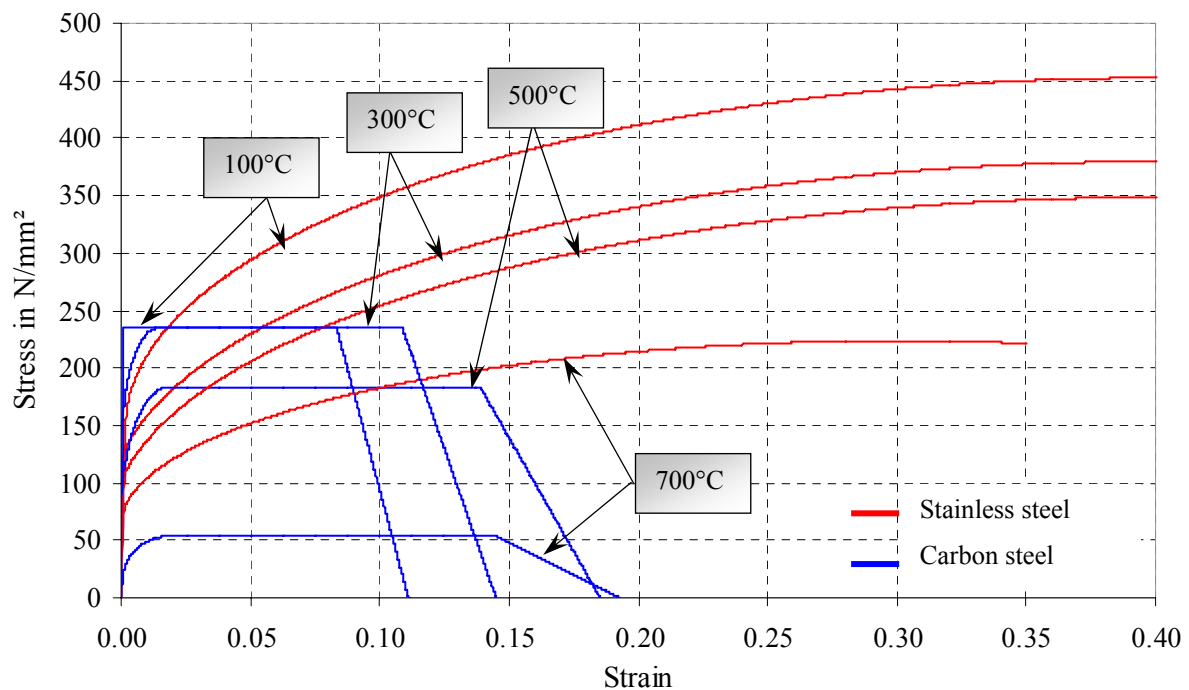
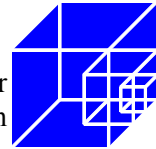


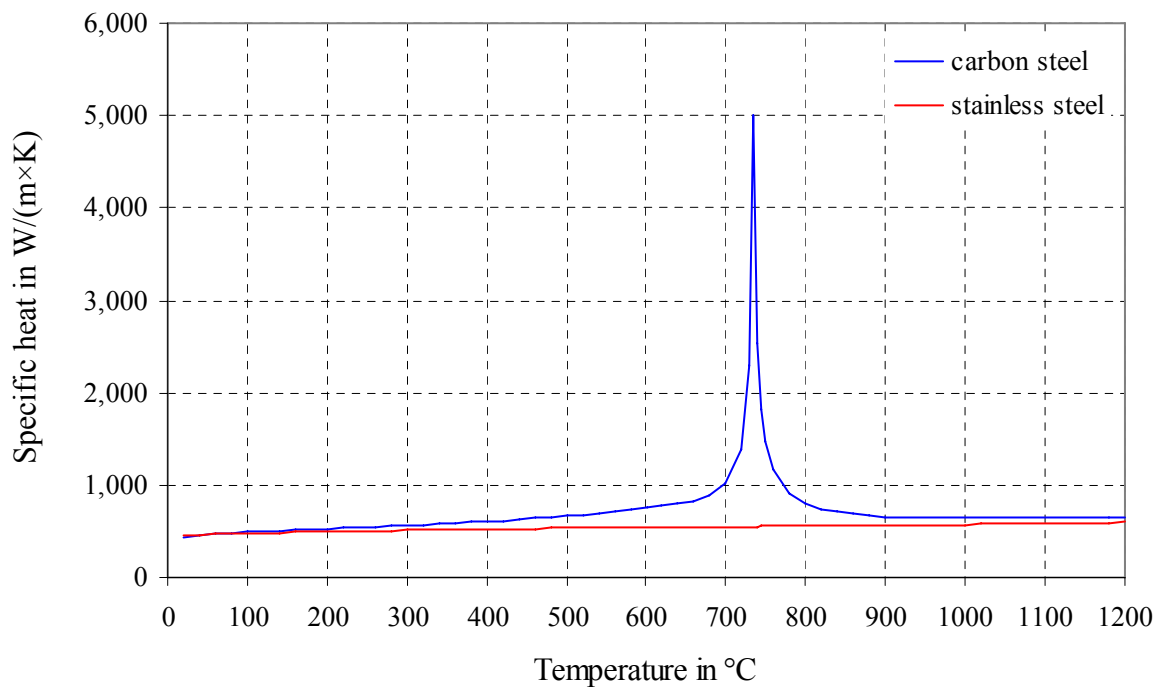
**Figure 3 Comparison of stress-strain relationship at elevated temperatures**

### 5.2.3 Thermal properties

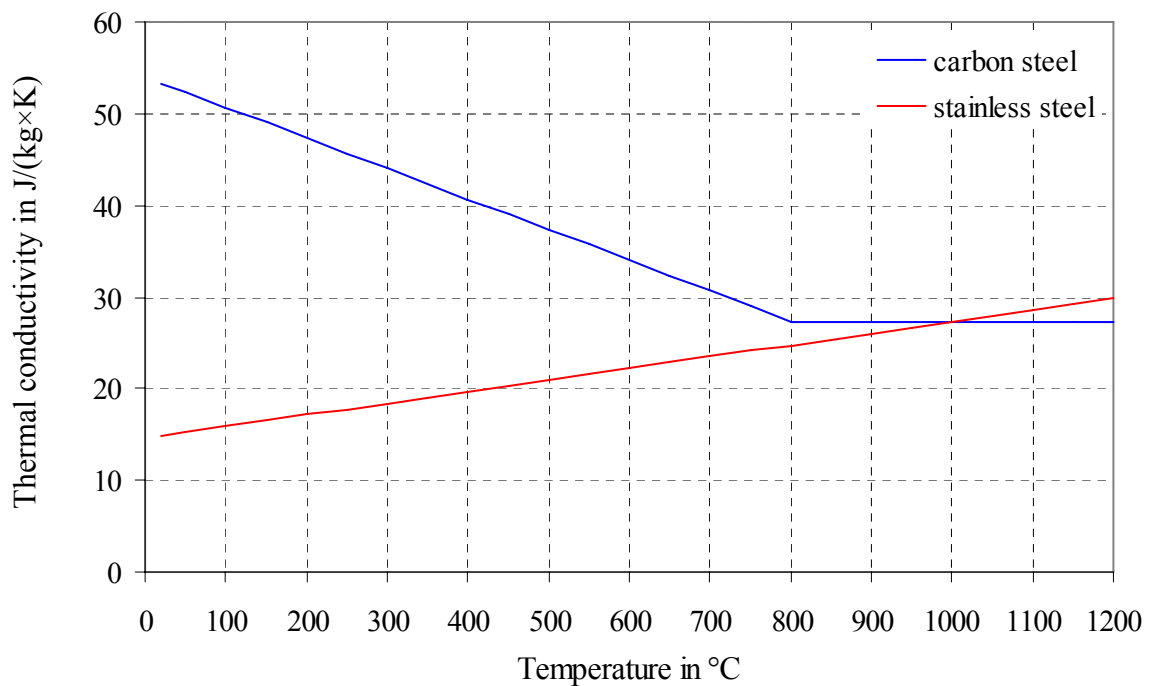
Specific heat is shown in Figure 4 for stainless and carbon steel. Both steel grades show comparable order of magnitude except for temperatures about 735°C, where specific heat of carbon steel increases exceedingly.

Figure 5 presents thermal conductivity of both materials. With rising temperatures thermal conductivity rises for stainless steel whereas it declines for carbon steel up to temperatures of 800°C. In the range between 800°C and 1,200°C a constant value is assumed for carbon steel so that conductivity is similar to that of stainless steel. Due to the far higher initial thermal conductivity, carbon steel heats faster than stainless steel in the initial stages of a fire.

Finally, the course of elongation depending on temperature is exhibited in Figure 6. It can be seen that stainless steel is subdued to higher elongation than carbon steel. This should be considered in the design of connections.



**Figure 4** Comparison of specific heat at elevated temperatures



**Figure 5** Comparison of thermal conductivity at elevated temperatures

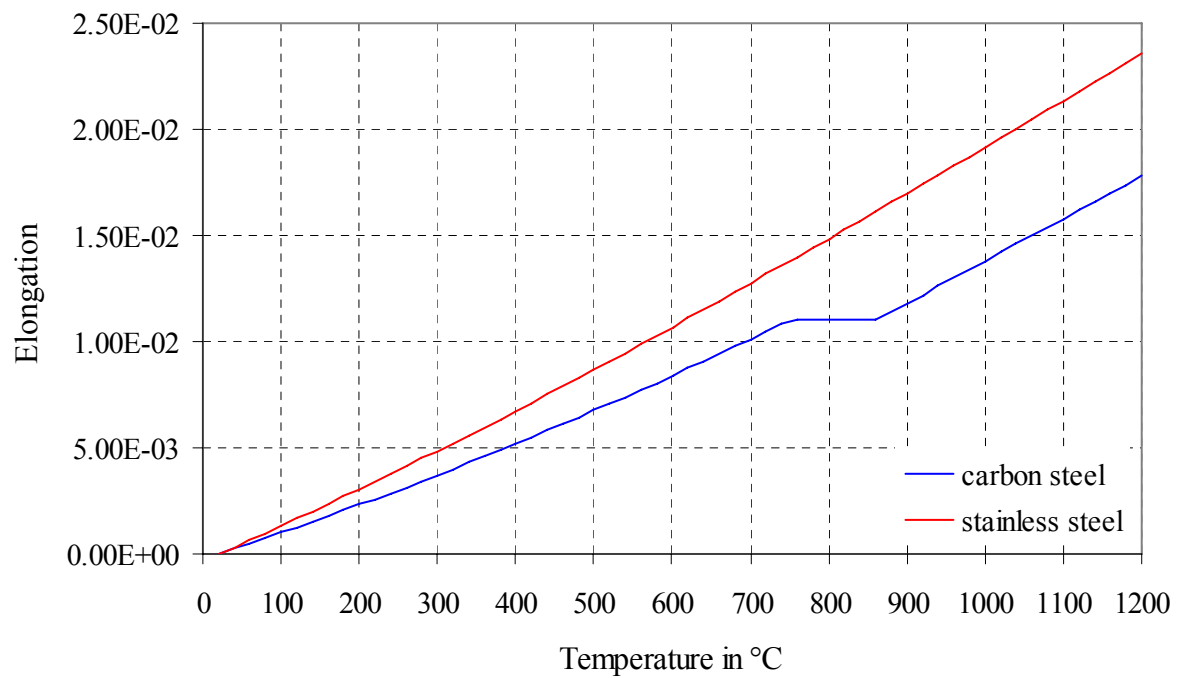
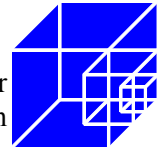
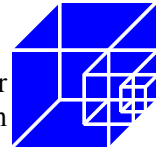


**Figure 6** Comparison of elongation at elevated temperatures



## 5.3 Separating members

### 5.3.1 Task and introduction

A new type of laser-welded stainless steel slab panel with rock wool insulation has been developed by Kenno Tech Ltd. In the frame of this project, investigations have been carried out by the Leibniz University Hannover (LUH), Germany in cooperation with VTT, Finland, to prove that a fire resistance of 30 to 60 minutes can be achieved without additional active or passive fire protection.

VTT performed two fire tests on the specimen and additional thermal analysis with a two-dimensional FE-model in COMSOL Multiphysics. It was task of LUH to develop a Finite-Element Model for thermal as well as mechanical analysis including nonlinear material behaviour at elevated temperatures. Therefore the software ABAQUS has been used. The ABAQUS results of temperatures and deformations have been compared to results of fire tests and of numerical calculations performed by VTT.

### 5.3.2 Geometry of the test specimen

The following information was provided by VTT:

- Insulated slab panel in office building, cross-section of floor structure (see Figure 7)
- Loading: Live load  $250 \text{ kg/m}^2$  ( $2.5 \text{ kN/m}^2$ ) for normal temperature design
- Material: Stainless Steel grade EN 1.4301
- Thermal insulation: Blowing rock wool  $75 \text{ kg/m}^3$  to  $115 \text{ kg/m}^3$
- Fire load: EN 1363-1: 1999 (ISO 834-1) at exposed side

The test specimen consists of two elements. The size of each element is  $4300 \text{ mm} \times 1505 \text{ mm}$ . Each part is encircled with C-profiles ( $120 \times 20 \times 0.7 \text{ mm}$ ) and the C-profiles in the middle between the two parts are welded together (see Figure 8).

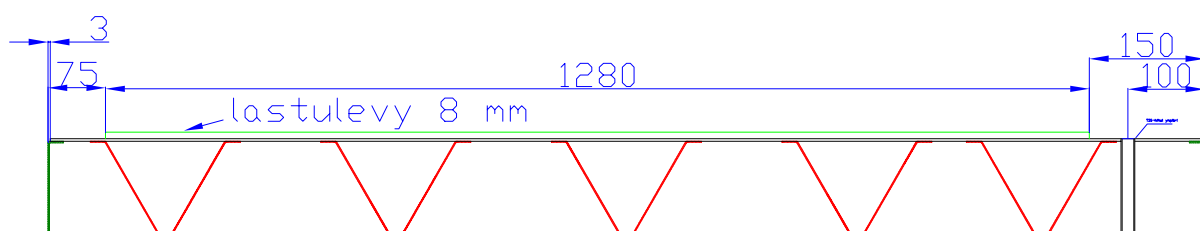


**Figure 7:** Cross-section of the slab panel „Kenno Tech floor“, test specimen (VTT)

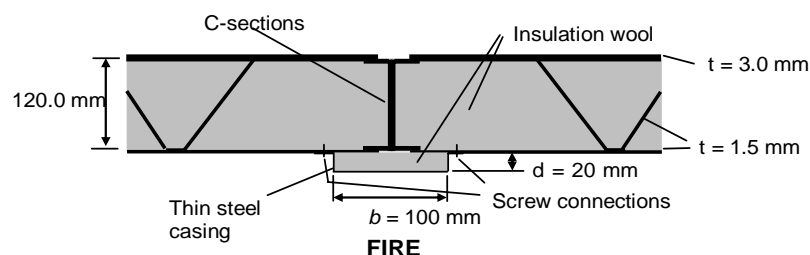
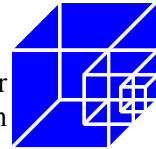


**Figure 8:** Connection of two test specimens



Geometry data of the cross section:

V-shaped steel profiles:  $h = 120 \text{ mm}$ ,  $t = 1.5 \text{ mm}$ ,  $\alpha = 60^\circ$ , AISI304  
Exposed side plate: 1.5 mm thick, AISI304  
Unexposed side plate: 3.0 mm thick, AISI304  
Total depth of floor: 124.5 mm

### 5.3.3 Material properties

#### Thermal material properties of insulation material

The density of the rock wool used in the fire tests was  $\rho = 115 \text{ kg/m}^3$ . However, corresponding thermal material properties for this type of rock wool were not available. But models for slabs with rock wool insulation of densities  $30 \text{ kg/m}^3$  (wool30) and  $140 \text{ kg/m}^3$  (wool140) had been determined by VTT on the basis of earlier tests, which were expected to define upper and lower bounds for the thermal calculations. The material properties provided by VTT are summarized in Table 1.

**Table 1: Thermal material properties for the insulation material**

mineral wool	$\rho$ [kg/m <sup>3</sup> ]	$c_p$ [J/(kg×K)]	$\lambda$ [W/(m×K)]
wool30	30	900	$\lambda = 0.034 - 0.00016 \times \theta + 1.09 \times 10^{-6} \times \theta^2$
wool140	140	800	$\lambda = 0.0341 - 0.0095 \times (\theta/100) + 0.0034 \times (\theta/100)^2$

### 5.3.4 Fire tests

#### VTT fire tests

VTT performed two fire tests at its laboratory: First, a small scale test with an unloaded specimen to analyse the thermal behaviour of the element and in a second step a large scale test with full dimensions of the specimen. Variable loads for the analysis of the load-bearing characteristics were applied. Both test specimens were exposed to standard fire from the bottom side.

#### Small scale fire test

VTT performed a small scale fire test on an unloaded Kenno Tech floor element in September 2005 [5]. The slab element had the original cross-section but was reduced in length and width to dimensions of  $1250 \times 1250 \text{ mm}$ . The test specimen was heated from below according to standard fire curve. The test setup is shown in Figure 9 with the arrangement of thermocouples on the left side and view in the furnace on the right. Temperature plots as well as sketches for the detailed arrangement of the thermocouples can be found in [6].

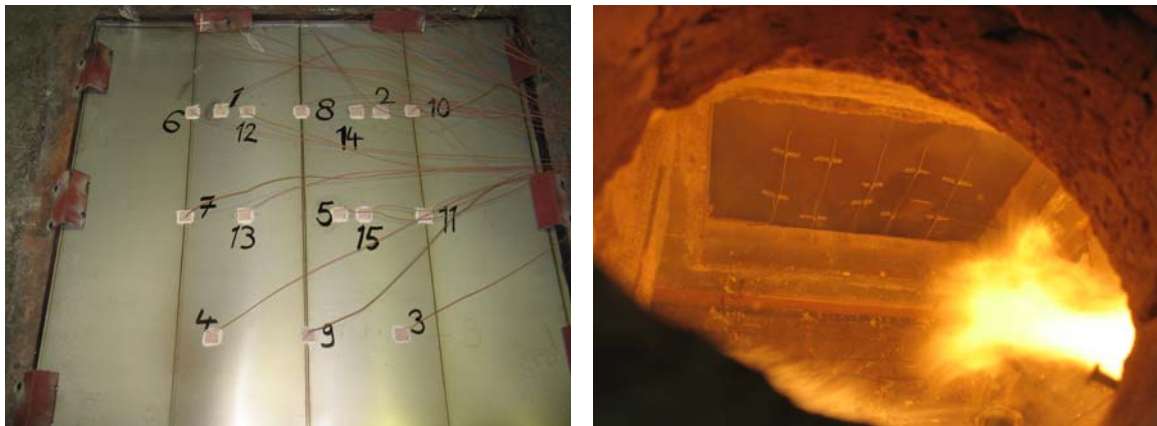
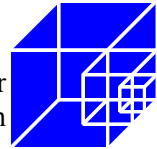


**Figure 9:** Test setup for the small scale fire test [6]

### Large scale fire test

VTT performed a large scale fire test on a loaded Kenno Tech floor element in November 2005. The tested member had original dimensions. The slab element was loaded with distributed variable load of  $p = 124 \text{ kg/m}^2$  as shown in Figure 10. Afterwards the loaded specimen was exposed to standard fire from the bottom side.

Unfortunately, the fire test had to be stopped after 47 minutes. Several cavities in the area of blowing mineral wool led to high temperatures on the unexposed side of the test specimen as it can be seen in Figure 10.

Some information about the temperature development in the specimen is published in [6]. Furthermore, some data concerning temperatures and deflections have been provided by VTT in advance to the LUH for their investigations.



**Figure 10:** Large scale test at VTT laboratories: test setup, loading and caves of insulation material (taken from [6])



### 5.3.5 Finite Element Models

#### FE-model for thermal analysis

The thermal action is applied according to the standard temperature-time curve.

$$\theta_g = 20 + 345 \times \log_{10}(8 \times t + 1) \quad (3)$$

$\theta_g$  gas temperature in the fire compartment [°C]  
t time [min]

The coefficient of heat transfer due to convection is applied according to EN 1991-1-2:

$$\alpha_c = 25 \text{ W/m}^2\text{K} \quad (\text{fire exposed side})$$

$$\alpha_c = 9 \text{ W/m}^2\text{K} \quad (\text{protected side})$$

The surface emissivity of the member is applied in accordance with all other project partners (see minutes of the project meeting in Ascot, UK, 22<sup>nd</sup> November 2005):

$$\varepsilon_m = 0.2 \quad (\text{fire exposed side})$$

Thermal analysis was performed as two-dimensional FEM-calculation with ABAQUS. For the transient heat transfer analysis DC2D4 DC2D3 elements were used and direct heat transfer was assumed between stainless steel and insulation material.

Only one half of the rib was modelled to reduce the size of the model. Geometry, mesh and boundary conditions for the calculation are illustrated in Figure 11.

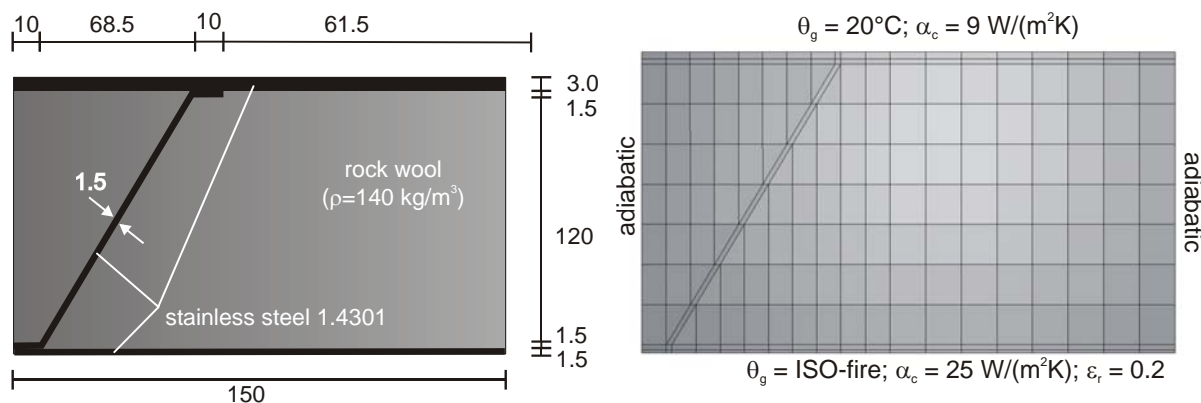


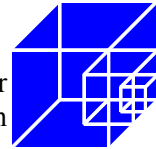
**Figure 11: Geometry and mesh of the thermal model**

#### FE-model for mechanical investigations

Only a small part of the slab element was implemented to reduce the size of the model and hence the required calculation time. The model represents one half of a rib because the V-profiles of the Kenno Tech element cause a one-way spanning load-bearing behaviour. The load-carrying in transverse direction is negligible.

Figure 12 shows a drawing of the structural element provided by VTT, which was the basis for model development. The region that was modelled in ABAQUS is marked in black borders.





Finally the dimensions of the numerical model can be seen in Figure 13 for the cross-section (left) and the longitudinal direction (right) of the slab. A small cantilever arm was modelled as well to adapt the correct testing conditions of the large scale test.

To consider the connection between the modelled part and the rest of the structural element the correct boundary conditions had to be applied as it is shown in Figure 13. The edges of the upper and lower sheets are continuously restrained for bending around the x-axis and in the middle of the two sheets the rib was fixed against horizontal displacement in y-direction. The rib is separated at midspan in longitudinal direction. Only one half was modelled to improve the symmetry of the slab-element acting as single-span beam. At the support all nodes of the web were fixed in z-direction. At midspan, all nodes of the cross-section were restrained for bending around the y-axis and fixed against horizontal displacement in x-direction.

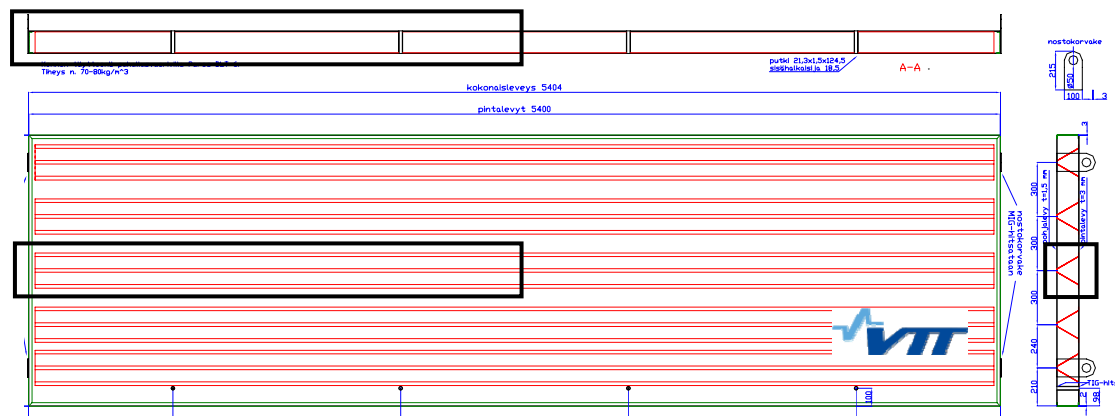


**Figure 12: Drawing of the test specimen (VTT)**

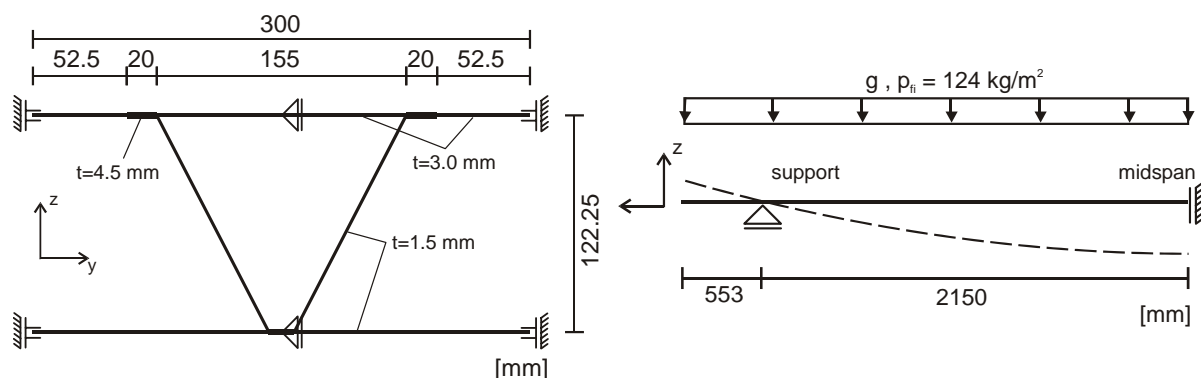
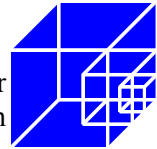


**Figure 13: Dimensions of the ABAQUS-model;  
Continuous boundary conditions along the edges (left) and at the ends of the rib (right)**

Shell elements with reduced integration S4R were used to model the slab panel. The corner radius of the steel plates was neglected. Thus the upper and lower flanges are continuous plates, where the thickness in the overlapping welding zones was taken as the sum of the thickness of the clinging plates. The distance of the planes, which were set by the upper and lower sheet, was 122.5 mm.



The numerical mesh and the applied boundary conditions are presented in Figure 14.

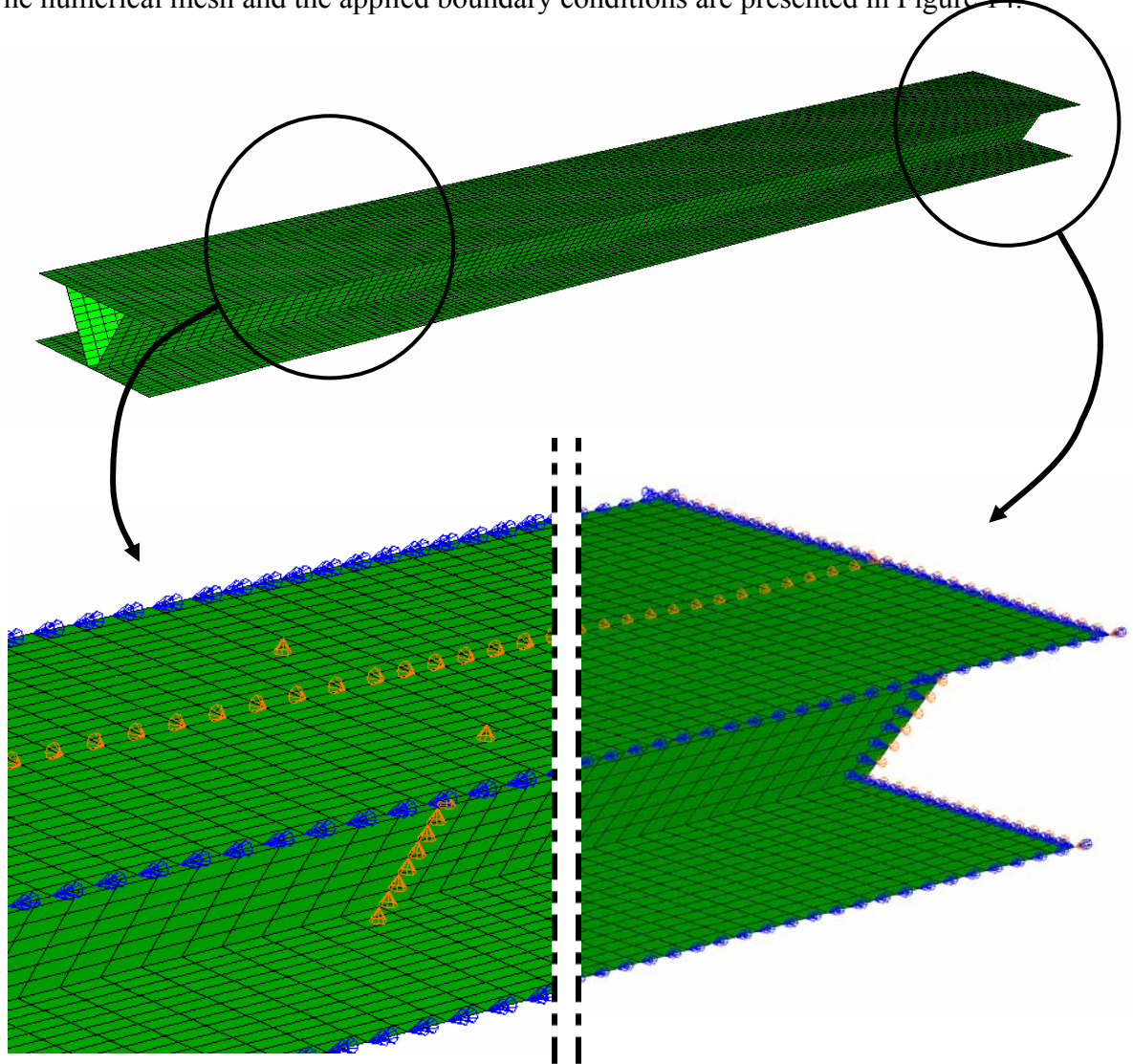


**Figure 14: Mesh of the slab panel (FE-Model ABAQUS) and boundary conditions**

### 5.3.6 Procedure at elevated temperatures

The aim of the mechanical analysis was the determination of the load displacement curve of the slab panel as described in the former chapter. Thermal action according to ISO-fire was considered. Thus a static analysis had to be performed taking the temperature variation and geometrical nonlinearities into account.

For a realistic estimate of the load-bearing capacity geometric imperfections had to be considered in the analysis. The imperfections were simulated superposing the FE-Model with the scaled buckling mode shape. The buckling mode shape was determined in a linear eigenvalue analysis. The base state for the eigenvalue buckling prediction was determined from a static, geometric nonlinear analysis considering the nonlinearities of the material as well. The base state was determined for different temperature fields at respective time steps. Hence, field variations of the temperature and consequently differences of the stiffness were considered, whereas residual stresses were neglected (no time-history).



The static analysis was then performed in two steps. In the first step the stresses and deformations of the static analysis of the imperfect model at room temperature were determined.

In the second step the time depending temperature field was applied. Therefore the maximum temperatures of the heat transfer analysis or the fire test results were assigned to respective node sets. Hereby the temperature variation in longitudinal direction of the slab panel was assumed to be constant. The time history of the temperatures was considered by the load history defined for each temperature node set. The so loaded slab panel was calculated taking large deformations into account.

During the analysis numerical instabilities emerged. For these unstable problems ABAQUS provides a tool to obtain a quasi-static solution. The numerical stability was obtained activating viscous forces, which are large enough to prevent instantaneous buckling, but small enough to not affect the behaviour significantly while the problem is stable. For this analysis, this tool was activated including the parameter STABILIZE.

#### **Temperatures of small scale fire test**

Due to the problems at the large scale test it was proposed by VTT to take the temperatures measured in the small scale test as basic temperatures for the mechanical analysis with ABAQUS.

The arrangement of thermocouples of the small scale fire test is shown in [5]. The temperatures applied to the ABAQUS-model were taken from a data file provided by VTT. The cross-section of the numerical model has been divided into 15 parts with different temperature sets. Every node has the same temperature development within each part.

The upper sheet was divided symmetrically in four parts as shown in Figure 15: edge, flange, flange-centre and centre. For the lower sheet a uniform temperature was applied over the whole width. The temperatures for the upper and lower sheet were taken as constant average values from the different measuring points along the length of the slab element.

Only one temperature-value was available in the web from the test. A continuous temperature distribution along the height of the web was established by nine additional temperatures interpolated linearly. The implemented temperatures are shown in Figure 16.

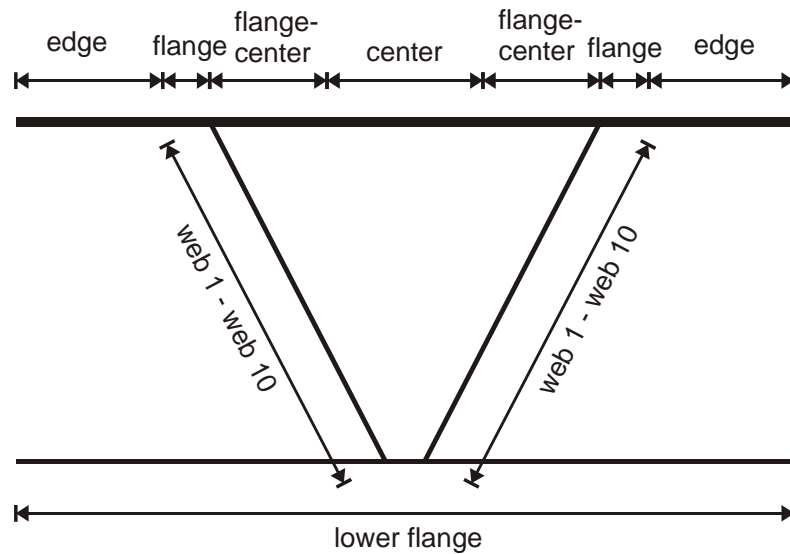
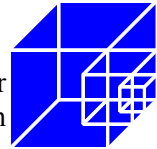


**Figure 15: Temperature sets for the numerical study**

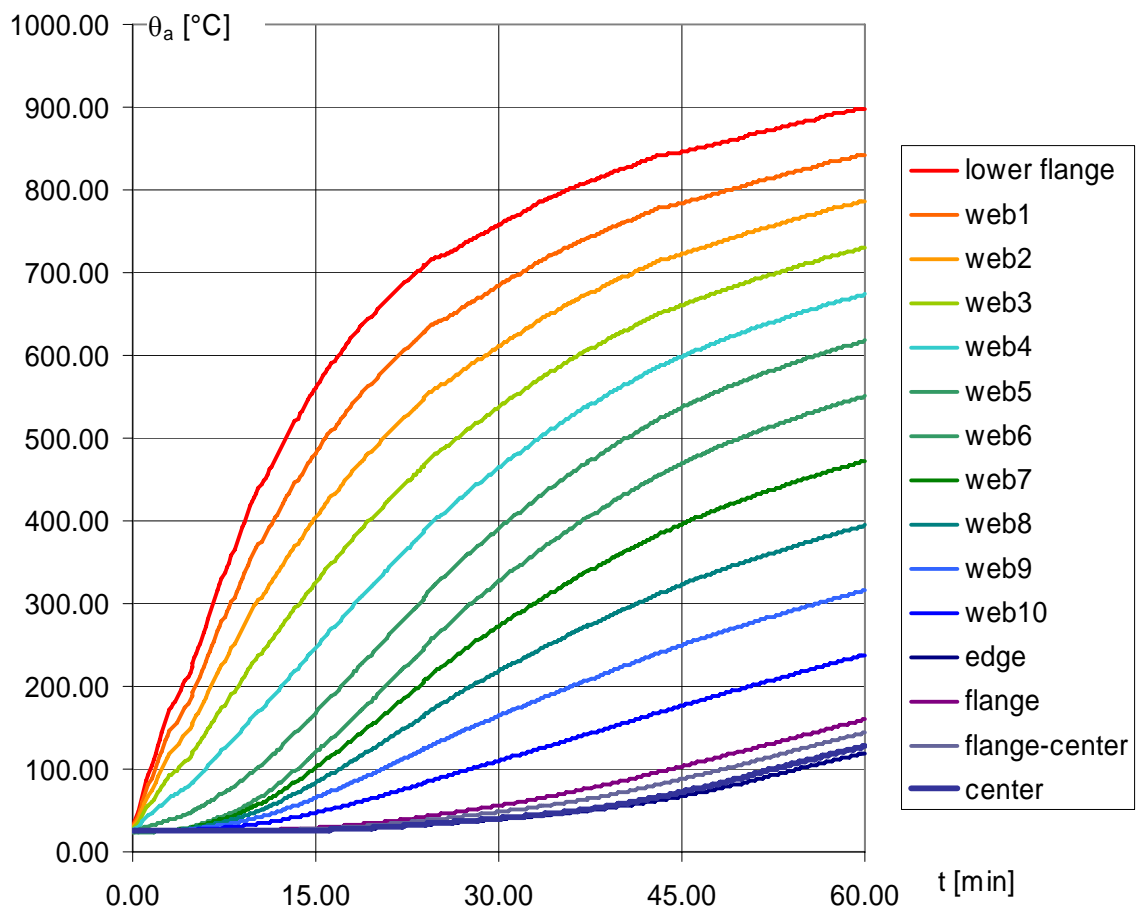
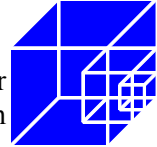


**Figure 16: Steel temperatures implemented in the ABAQUS-model (provided by VTT: small scale fire test)**



### 5.3.7 Results

#### Investigations at ambient temperatures

The cantilever arms, as they appeared in the large scale fire test, are neglected during investigations at ambient temperatures. The aim was to determine the load ratio in the fire situation to classify the loading in the large scale test so that the cantilever arms were negligible. The slab panel was considered as single span beam.

#### Determination of load ratio

According to EN 1993 3-1-2 the following load ratio has been defined:

$$\mu_0 = \frac{E_{fi,d}}{R_{fi,d,0}} \quad (5)$$

with:

$E_{fi,d}$  the design effect of actions for the fire situation;  
 $R_{fi,d,0}$  the corresponding design resistance in the fire situation for time  $t = 0$ .

#### Mechanical Action

The mechanical action on the member during the fire test was given by VTT:

Live load:  $p = 125 \text{ kg/m}^2 = 0.00125 \text{ N/mm}^2$

Dead load:  $g \approx 50 \text{ kg/m}^2 = 0.0005 \text{ N/mm}^2$

Regarding the accidental design situation of EN 1990 with  $\gamma_{GA} = \gamma_Q = 1.0$  the total action was calculated to:

$$E_{fi,d} = q = p + g = 175 \text{ kg/m}^2 = 0.00175 \text{ N/mm}^2$$

#### Load-bearing capacity at time $t = 0$ with simplified calculation methods

According to EN 1993-1-5, section 5.5.2 the cross-section of the Kenno Tech element was classified as follows:

$$\varepsilon = \left[ \frac{235}{f_y} \frac{E}{210000} \right] = 1.03 \text{ (stainless steel 1.4301)}$$

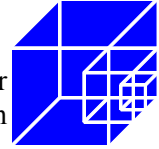
Upper sheet:

$$c/t = 155/3.0 = 51.6 > (c/t)_{\lim} = 30.7 \times 1.03 = 31.6 \text{ Class 4}$$

Web:

$$c/t = 140/1.5 = 93.3 > (c/t)_{\lim} = 74.8 \times 1.03 = 77.0 \text{ Class 4}$$

With respect to the buckling behaviour of compression cross-section parts the load-bearing capacity at time  $t = 0$  was calculated as elastic stress verification considering effective cross-section according to EN 1993.



EN 1993-1-4, section 5.2.3 gives rules to define effective widths for class 4-cross sections. The slenderness of the upper sheet led to an effective cross-section as it is shown in Figure 17. The web remained unreduced.

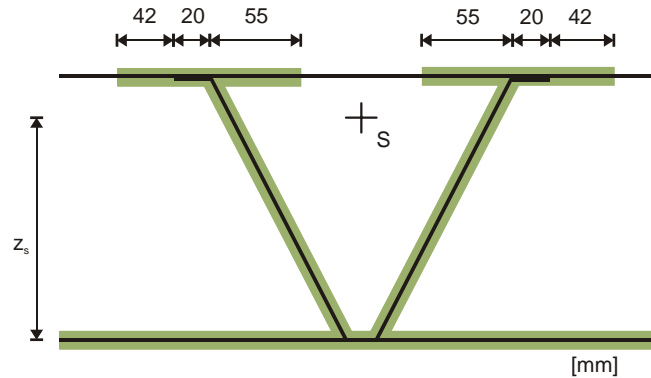


**Figure 17: Effective cross-section at time  $t = 0$  according to Eurocode 3**

Elastic cross sectional parameters were determined for the cross-section presented in Figure 17:

$$z_s = 71.7 \text{ mm}$$

$$I_z = 5.017 \times 10^6 \text{ mm}^4$$

With these parameters the bending moment capacity and finally the load-bearing capacity in the fire situation at time  $t = 0$  were calculated from the elastic stress verification.

$$M_{fi,Rd,0} = \frac{f_{y,k}}{\gamma_{M,fi}} \times \frac{I_z}{z_s} = \frac{220}{1.0} \times \frac{5.017 \times 10^6}{71.7} = 1.538 \times 10^7 \text{ Nmm} \quad (6)$$

$$R_{fi,d,0} = q_{fi,Rd} = M_{fi,Rd,0} \times \frac{8}{b \times L^2} = 1.538 \times 10^7 \times \frac{8}{300 \times 4300^2} = 0.0222 \frac{\text{N}}{\text{mm}^2} = 2220 \frac{\text{kg}}{\text{m}^2} \quad (7)$$

As a result, the load ratio was calculated according to equation (5):

$$\mu_0 = \frac{E_{fi,d}}{R_{fi,d,0}} = \frac{175}{2220} = 0.079 = 7.9 \%$$

Based on this low load ratio a high fire resistance time could be expected. The elastic deflection at midspan of the single span beam was calculated as:

$$w_{el} = \frac{5}{384} \times \frac{q \times b \times L^4}{EI} = \frac{5}{384} \times \frac{0.0222 \times 300 \times 4300^4}{2 \times 10^5 \times 5.017 \times 10^6} = 29.5 \text{ mm} \approx \frac{L}{150} \quad (8)$$

### Numerical simulation at ambient temperatures

A load-bearing calculation at ambient temperatures has been performed to analyse the load carrying behaviour under increasing life loads and to verify the load ratio. The analysis has been carried out with the ABAQUS-model, which was described above considering material



and geometrical non-linearity and applied imperfections, which have been determined by linear buckling analysis at room temperature.

First, the dead load of the Kenno Tech element was applied and in a second step the life load was increased continuously up to twenty times the load of the VTT-fire test.

Figure 18 shows the deformed geometry of the slab panel with Mises-stresses and an extension of the midspan region with normal-stresses ( $\sigma_x$ ). Furthermore, the buckling behaviour of the compression zones can be observed (scale factor: 1.00, no amplification).

The diagram in Figure 18 shows the deflection of the member at midspan against life loading. The curve demonstrates that the load-bearing capacity determined by simplified calculation methods complies well with the numerical simulation. However, the comparison of the deflection shows that the numerical model is obviously softer at higher deflections than a simplified elastic calculation as a result of the non-linear material behaviour.

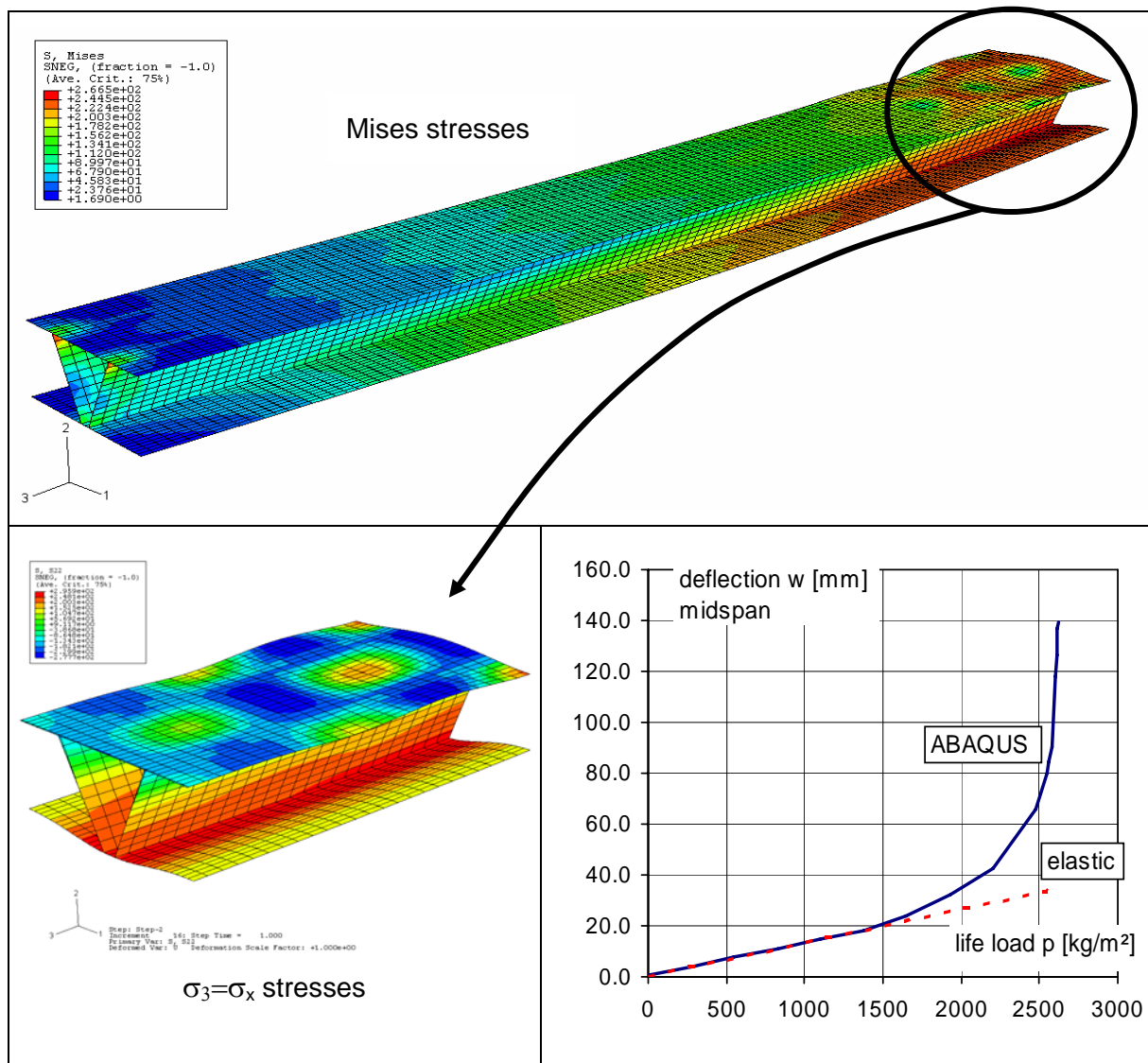
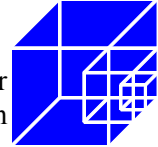


**Figure 18: Stresses and deformed geometry of the ABAQUS-model at normal temperature and load-deflection relation for increasing life load**





## Results of the thermal analysis

Thermal analysis has been done with the two-dimensional ABAQUS-model. The calculation was performed up to 60 minutes with standard fire heating from below. The two material properties wool30 and wool140 for insulation material were used as previously introduced.

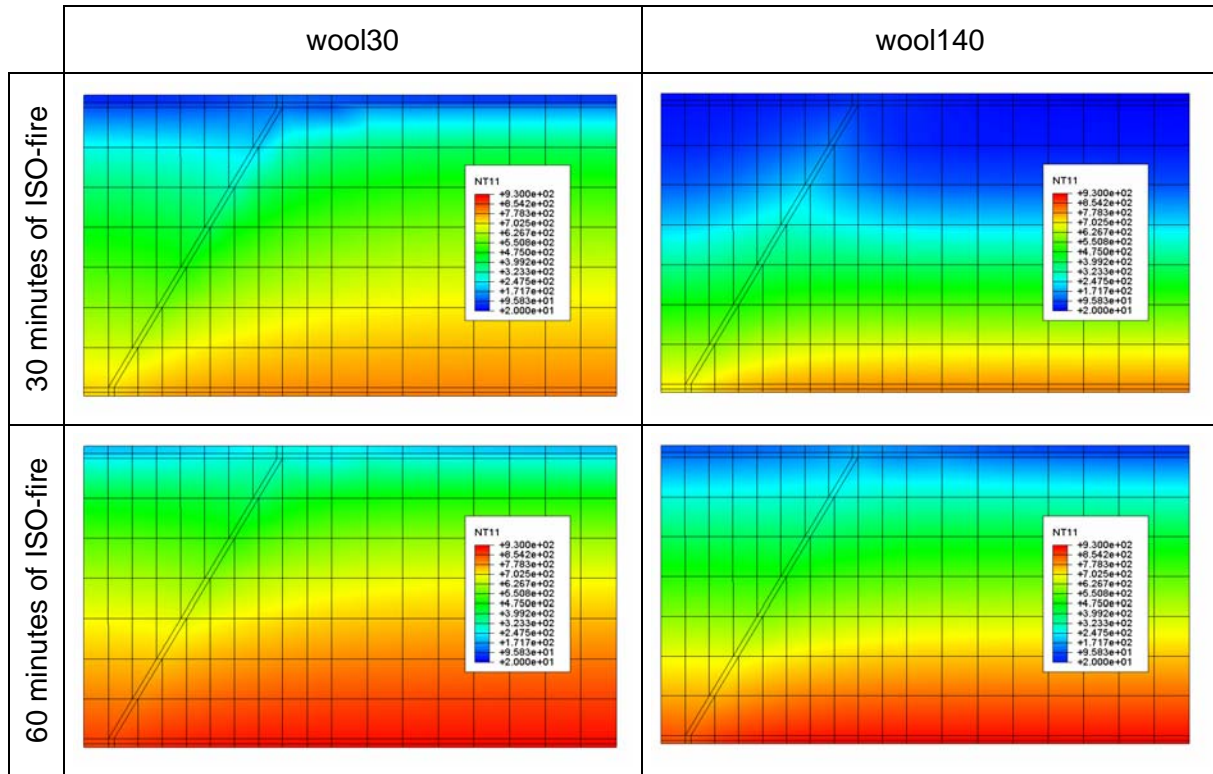


**Figure 19: Temperature plots for 30 and 60 minutes of standard fire with two insulation material wool30 and wool140**

The results of the calculation are shown in Figure 19 as temperature plots after 30 and 60 minutes of standard fire exposure. On the left side the results for wool30 and on the left side for wool140 are illustrated. Obviously the low density rock wool led to higher temperatures than wool140. Furthermore, the comparison of the two insulation materials shows that the application of the low density rock wool 30 led to slower heat flux in the area of the web than in the area of pure rock wool. This phenomenon can be explained by the thermal diffusivity  $a$ , which is defined in Eq. (9)

$$a = \frac{\lambda}{c \times \rho} \quad \left[ \frac{\text{mm}^2}{\text{s}} \right] \quad (9)$$

The thermal diffusivity defines the diffusion of heat in a medium and depends on thermal conductivity  $\lambda$ , which is higher for steel than for the insulation material, as well as on density  $\rho$  and thermal capacity  $c$ . The thermal diffusivity is plotted in Figure 20 as a function of the material temperature for stainless steel and the two different rock wools. The comparison demonstrates that for temperatures higher than 400°C the values for wool30 are higher than





the values for stainless steel and high density rock wool, which leads to the effect shown in Figure 19.

The numerical results show that the temperature development in the member reacts sensitively on the material properties of the insulation material.

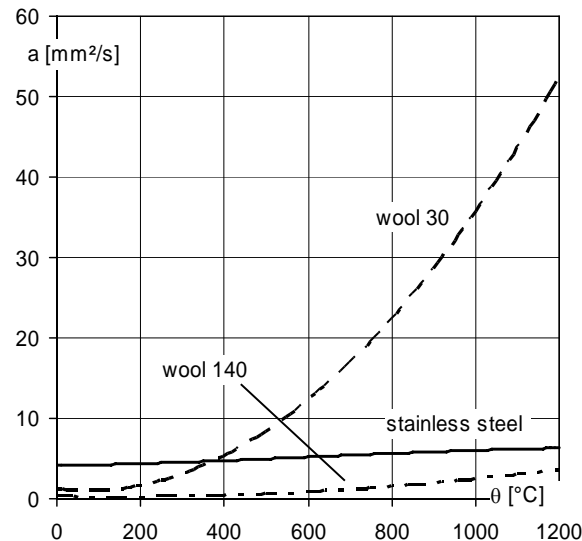


**Figure 20: Thermal diffusivity of stainless steel and low and high density rock wool against material temperature**

The results of the numerical analysis using COMSOL and ABAQUS were compared to the measured temperatures of the small and large scale fire tests and are illustrated in Figure 21. The temperatures are divided in three diagrams: for the upper flange of the steel profile (unexposed side), the middle of the web and the lower sheet (exposed side). All measured values that refer to the same part of the cross-section (e.g. lower sheet) but are disposed over the area of the test specimen are plotted in small dotted lines. An average value was calculated from these measured values and is shown as a thick line. The results of the numerical calculations are plotted for rock wool 30 and 140.

For the small scale test the comparisons show that the numerical calculations are conservative in relation to the average values of the measured temperatures. Furthermore, the results with high density rock wool lie closer to the measured values of the small scale test. Unfortunately, due to the problems in blowing rock wool installation, there is a lot of scatter in the results of the large scale test. This makes comparisons to calculations difficult and these results should be considered with caution. However, fairly good agreement between ABAQUS and COMSOL analysis results can be seen here as well.

When comparing the average temperatures of small and large scale tests it is obvious that the temperatures at the unexposed side are about 100 % higher in the large scale test, while the temperatures at the exposed side are nearly the same. These circumstances lead to different temperature gradients over the height of the member and this will be significant regarding the deflection.

The Eurocodes define insulation criteria for separating members: the temperature rise at the unexposed side of the member must not exceed 140°C as average and 180°C as peak value. The measured temperature results reveal that the insulation criterion I 60 is met in the small but not in the large scale test and the numerical calculations with wool140.

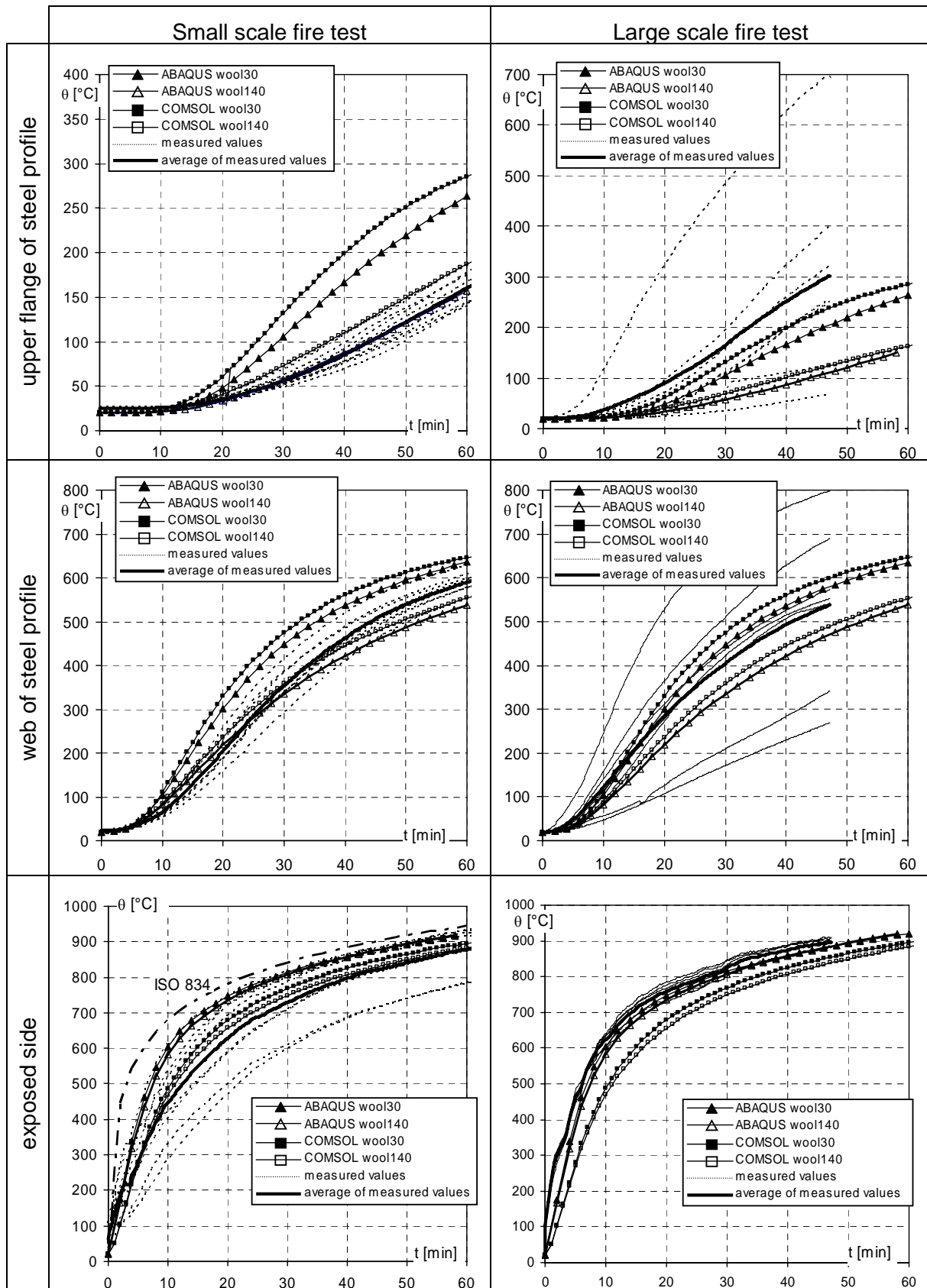
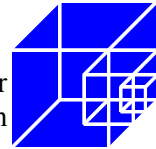
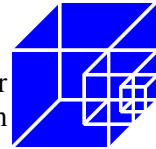


Figure 21: Comparisons between numerical calculations and measured temperatures from fire tests



## Results of the mechanical analysis

### Buckling Mode Shape - Imperfections

For the determination of the buckling mode shape a linear eigenvalue analysis was performed. Various calculations were performed applying different temperature fields.

$$\theta(x,y,z) \text{ } t = 0 \quad (\text{room temperature})$$

$$\theta(x,y,z) \text{ } t = 600 \quad (10 \text{ min})$$

$$\theta(x,y,z) \text{ } t = 3600 \quad (60 \text{ min})$$

The determination of the buckling modes was performed in accordance with the described procedure of report 1 [11], where further details can be found.

The chosen buckling modes for the application of imperfection is shown in Figure 22. The first eigenvalue was taken for the imperfect geometry at the compression zone at midspan in the upper sheet and the ninth eigenvalue for the compression at the support in the lower flange.

A common value for the magnitude of the imperfection was applied as:

$$\omega = b / 200 = 155.0/200.0 = 0.775 \text{ mm}$$

The buckling mode shape according to Figure 22 was scaled with  $\omega$  and superposed to the perfect geometry. The nonlinear geometric calculations were performed taking into account imperfect geometry.

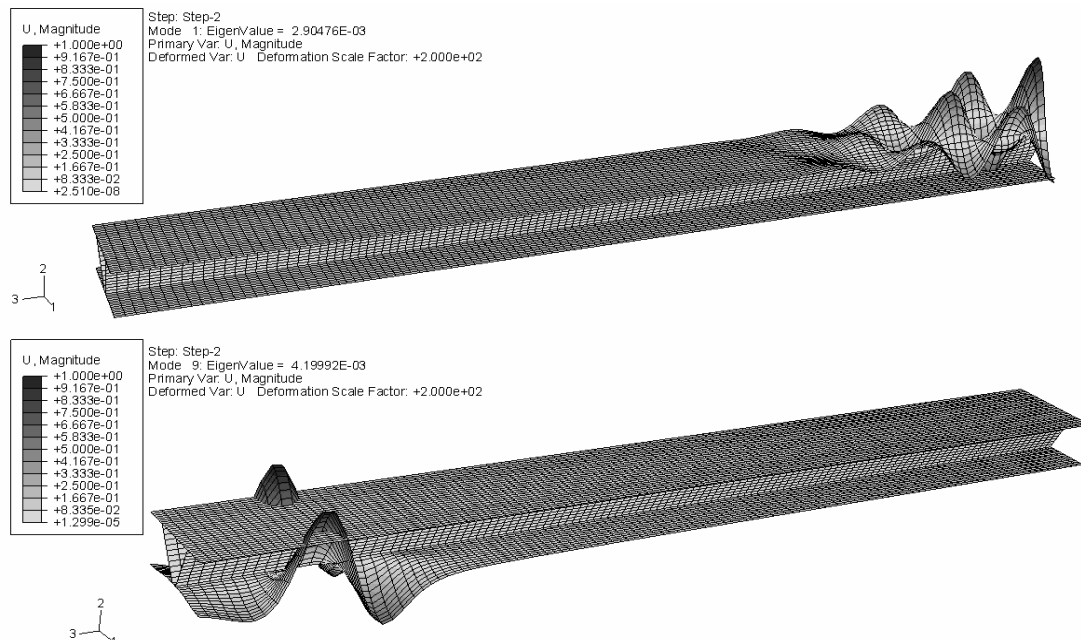


**Figure 22: Buckling modes for the two compression zones at midspan and at support**

### Load-bearing behaviour of the slab panel subjected to ISO-fire

Finally the slab panel with the imperfect geometry was subjected to the temperatures which were determined in the small scale fire test. The deformed shape after 60 minutes of standard fire is presented in Figure 23. The contour-plot of the model shows Mises-stresses.

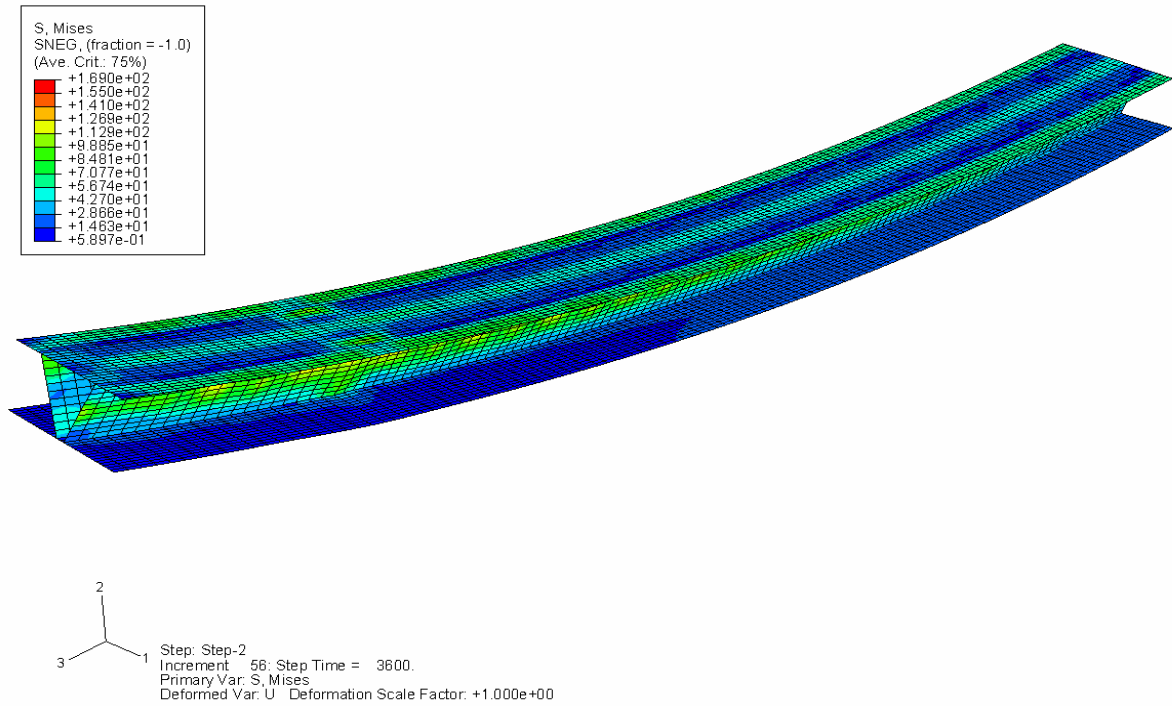
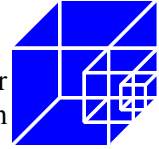


**Figure 23: Mises stresses on the deformed slab panel after 60 min of ISO fire**

The node at midspan and at the end of the cantilever arm at the lower sheet in the middle of the two webs was chosen as reference node for the time-displacement curve in Figure 24. In addition to the vertical deflection resulting from the numerical simulation, the measured values from the large scale fire test is plotted in the diagram on the left side of Figure 24.

The comparison of numerical and measured results shows that the deflection obtained with ABAQUS are much higher than in the fire test. Although very large deflections can be observed ( $w > 250 \text{ mm} \approx L/20$ ) it seems from the numerical analysis that a quasi steady state of deflections remains between 45 and 60 minutes. No failure occurs.

Thus, to interpret the appearing deflections, the thermal bowing is determined simplified from Eq. (10), as the temperature gradient  $\Delta\theta$  is calculated with the average temperatures of the upper and lower sheet. The results of Eq. 10 and Eq. 11 are depicted in Figure 25 as well, with both the temperatures from the small and large scale test.

$$w_{\theta,m} = \frac{L^2}{8} \alpha_T \frac{\Delta\theta}{d} \quad (10)$$

$$w_{\theta,c} = \frac{L_c}{2} \alpha_T \frac{\Delta\theta}{d} \cdot (L + L_c) \quad (11)$$

with:

- $d$  distance of the upper and lower flange;
- $\Delta\theta$  temperature gradient;
- $\alpha_T$  expansion coefficient;
- $L$  span between supports;
- $L_c$  span of the cantilever arm.

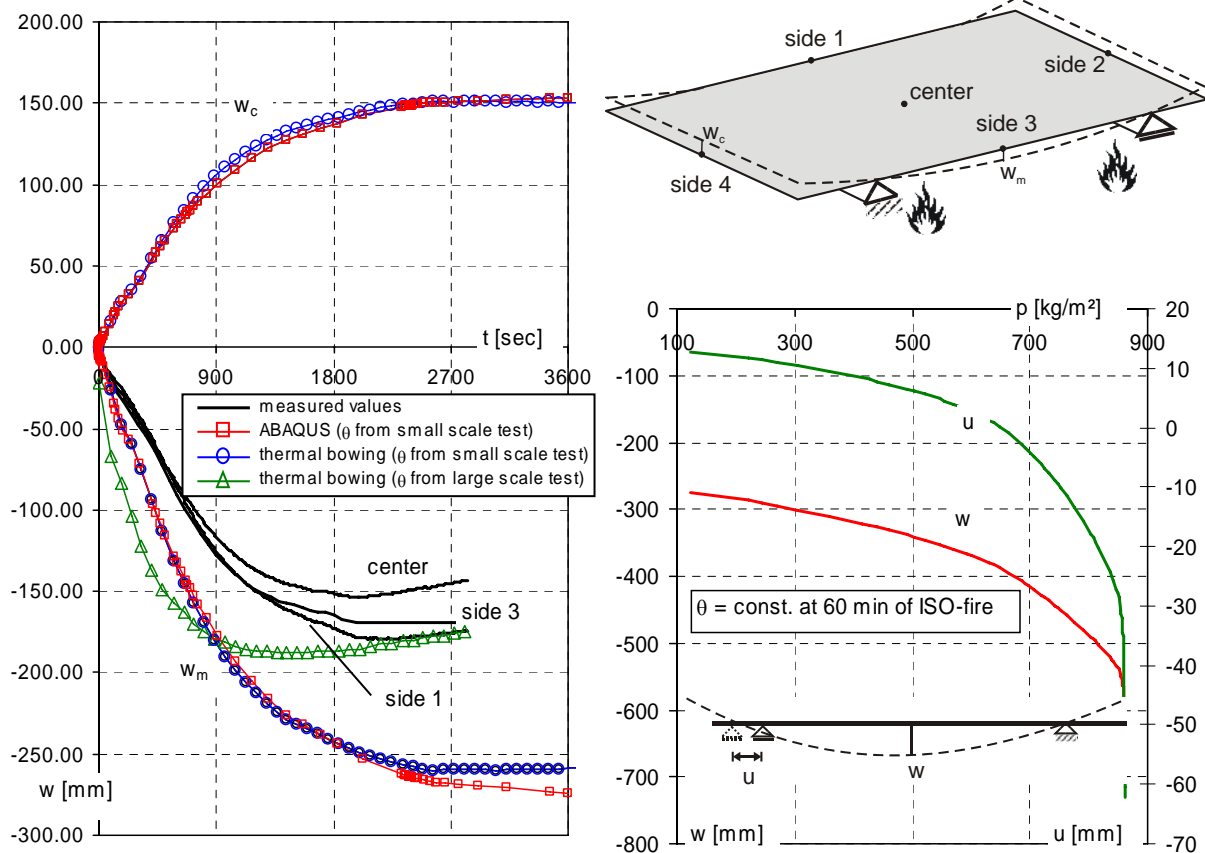
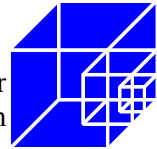


**Figure 24: Vertical displacement due to heating of the member against time (left); Vertical displacement due to load increasing against variable loads (right)**

Obviously, the total deflection during 60 minutes of ISO-fire in ABAQUS is governed by thermal bowing, and not by the effects of the mechanical loads and the loss in bending stiffness due to high steel temperatures. The reason for the differences between the test and the numerical analysis is the application of small scale fire test temperatures on the numerical model because those values differ from the temperatures measured in the large scale test. Therefore the thermal bowing determined from the large scale temperatures are plotted in Figure 24 as well. The maximum deflection obtained fits well with measured values of the large scale test. As a result of the insulation cavities the temperatures of the upper sheet were higher in the large then in the small scale test. Assuming that the temperatures of the lower sheet remained nearly the same, the thermal gradient  $\Delta\theta$  and consequently the deflections obtained from thermal bowing were smaller.

Overall, the deflections show that the requested fire resistance of 60 minutes for load-bearing capacity was reached and failure did not occur. For this reason, a load-bearing calculation was performed following the heating of 60 minutes of ISO-fire with constant temperatures and increasing live loads. The results for the deflection at midspan and the horizontal displacement at support are plotted on the right side of Figure 24. The deformed slab model at ultimate limit state is presented in Figure 25. Buckling of the lower sheet at the support and of the web at midspan can be observed.

An ultimate load  $p \approx 750 - 800 \text{ kg/m}^2$  for the structural member can be estimated from the graphs of Figure 24 for R 60 due to rapidly increasing deflections which complies with a load



ratio of  $\mu_0 = 0.35$ . According to the ABAQUS-analysis a deflection of about 50 cm at midspan and a horizontal displacement less than 2 cm at support have to be expected within this live load. However, the large deflections due to thermal bowing may define a lower limit state for serviceability.

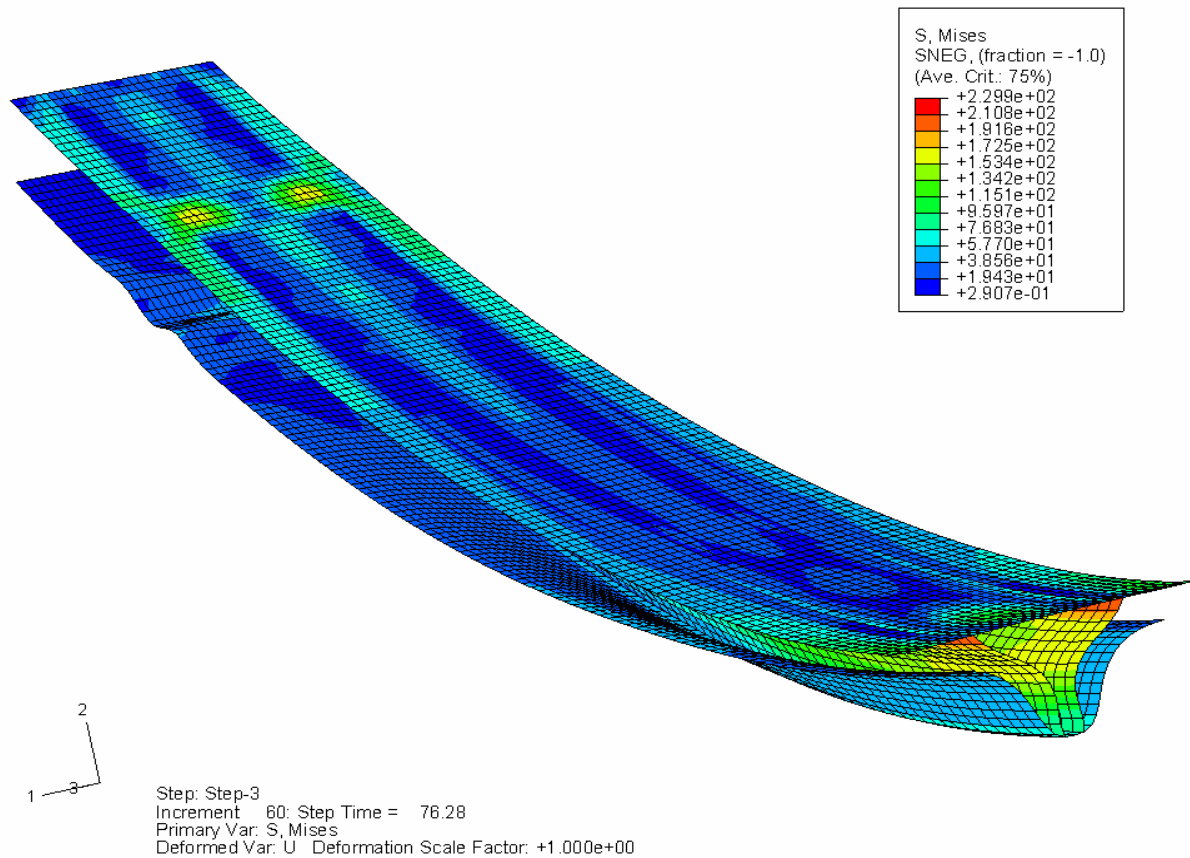


**Figure 25: Deformed shape with Mises stresses at ultimate limit state (no amplification)**





## 5.4 Load-bearing structures

Various stainless steel load-bearing structures are defined in [6], Tables 7.1 and 7.2 by VTT. Two promising cross-sections were taken from these to achieve fire resistance times of 30 or 60 minutes for unprotected or partially protected stainless steel load-bearing structures.

### 5.4.1 Nested tubes

#### Introduction

At first, the load-bearing behaviour of nested tubes exposed to ISO standard fire was investigated. The cross-section consists out of tubes within each other, where the space between the profiles is insulated with mineral wool. The space inside the inner profile is empty (see Figure 26). The cross-section was defined by VTT, which also provided data from thermal analysis and fire tests.

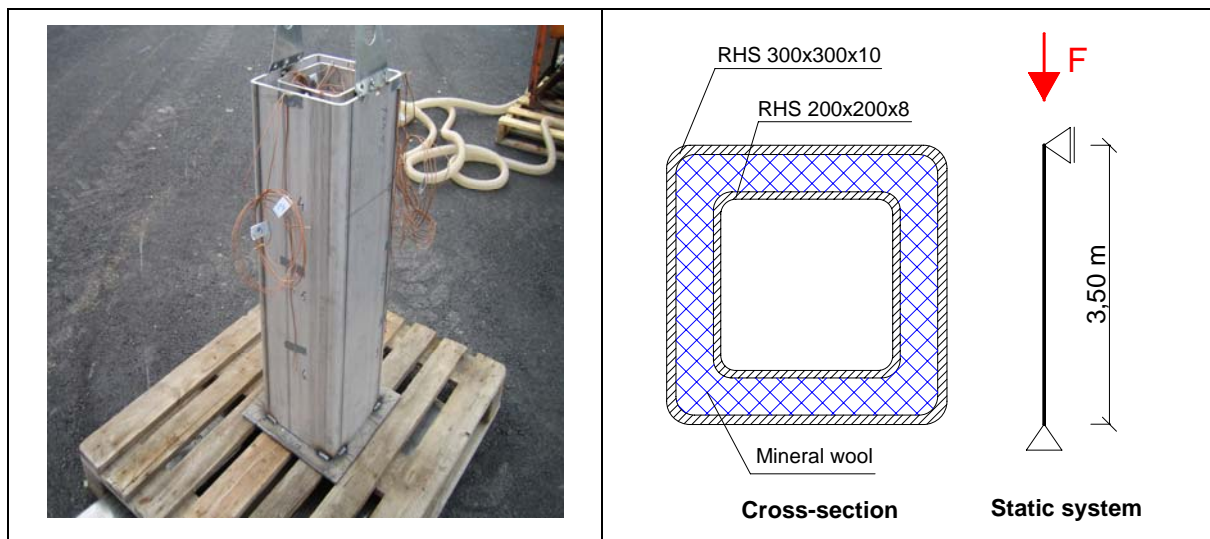


**Figure 26 Test specimen (VTT) (left), cross-section and static system (right)**

#### Thermal analysis

##### Comparison of different material properties for stainless steel

Gardner and Ng [7] proposed material properties for stainless steel which differ from those defined in EN 1993-1-2. The revised values are the emissivity with a value of 0.2 (in place of the currently assumed value of 0.4) and the heat transfer coefficient with a value of 35 W/(m<sup>2</sup>×K) (in place of the currently assumed value of 25 W/(m<sup>2</sup>×K)).

The density of wool is 75 kg/m<sup>3</sup>. As the thermal properties for the injected mineral wool were not available, thermal conductivity is assumed as follows:

$$\lambda = 0.034 - 0.00016 \times \theta + 1.09 \times 10^{-6} \times \theta^2 \quad (12)$$

Specific heat capacity is taken as 900 J/(kg×K).

To assess the effects of the revised stainless steel values, the above presented material properties were implemented in ABAQUS. On this basis, two-dimensional thermal analysis of the nested tubes cross-section was performed. Moreover, thermal analysis using the material properties of carbon steel was carried out to compare the different materials with respect to



their heating behaviour. All cross-sections were exposed to ISO standard fire. Resulting cross-sectional temperatures were measured at the corners of the outer and inner tube, which is denoted as measure points 1 and 2 in Figure 27.

As it can be seen in this figure, material properties for stainless steel according to Gardner result in low cross-sectional temperatures in comparison to the temperatures obtained from the use of material properties according to EN 1993-1-2. The maximum difference between these two material sets amounts to 54°C after 23 minutes exposure to ISO standard fire. After 30 minutes, the difference is slightly reduced to 47°C, whereas it is only 19°C after 60 minutes of fire exposure. In contrast to this, the corresponding differences are negligible for the inner tube, which is protected by mineral wool.

Regarding the outer tube, the comparison between the thermal analysis using the material properties according to Gardner and carbon steel shows maximum differences of 88°C after 16 minutes of exposure to ISO standard fire. However, this difference is reduced to only 11°C after 30 minutes due to the increased thermal capacity of carbon steel at cross-sectional temperatures about 735°C (compare Figure 4). Again, there are only slight differences regarding the inner tube.

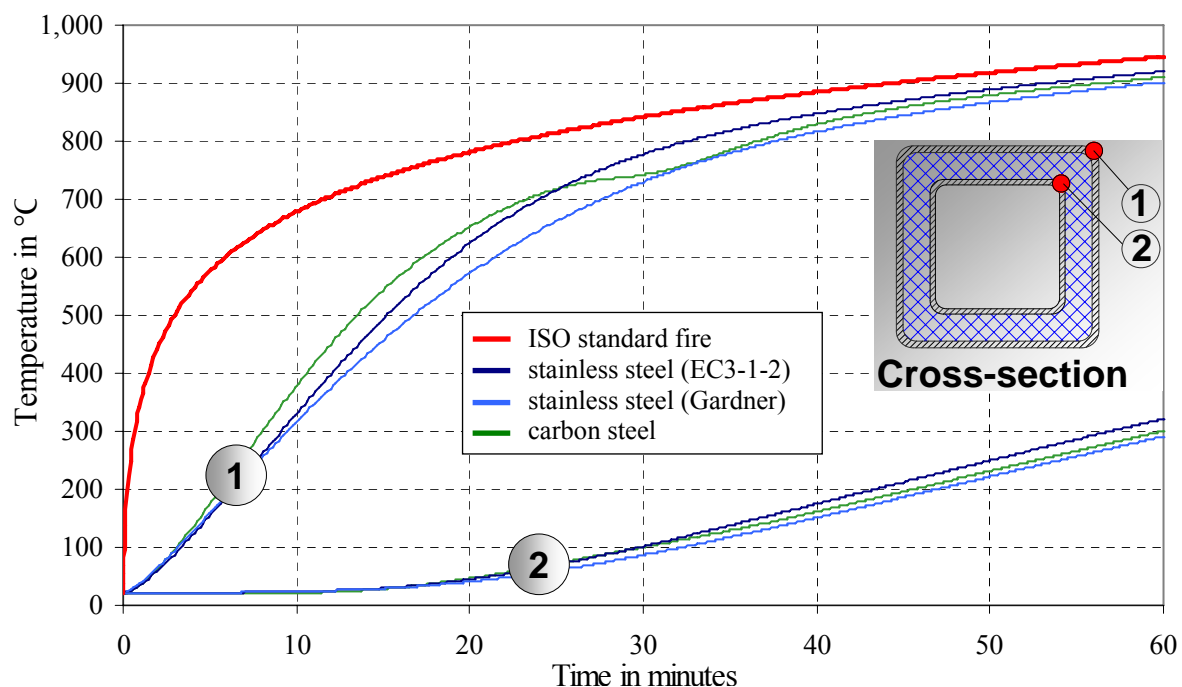


**Figure 27** Cross-sectional temperatures of nested tubes for varying material properties

It can be concluded that the use of revised material properties according to Gardner improves the fire resistance of stainless steel to a limited extent. This is in particular interesting for unprotected stainless steel load-bearing structures aiming at 30 minutes fire resistance. For following numerical investigations, material properties of stainless steel are taken into account according to Gardner.





### Comparison to test results

Partner VTT provided data from fire tests on unloaded nested tubes specimens. The dimensions as well as location and numbering of thermocouples is presented in Figure 28 (VTT):

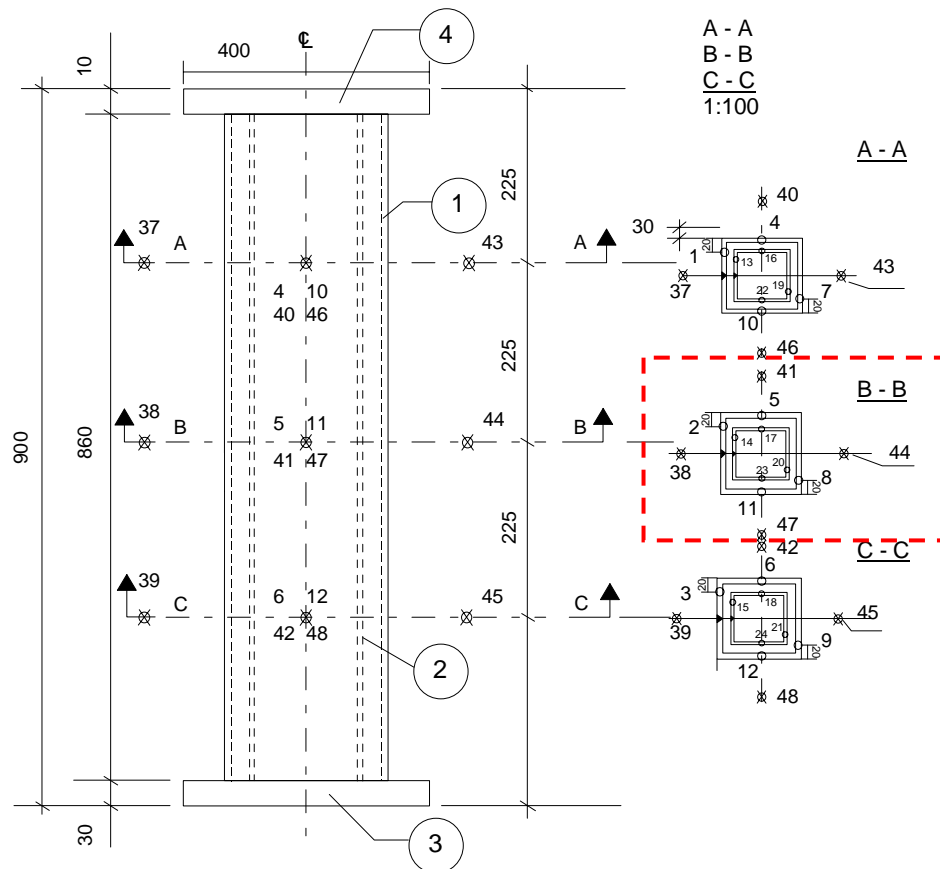


**Figure 28 Test set-up and cross-sectional details for nested tubes with fire protection (VTT)**

The gas temperature in the test carried out by VTT followed closely the ISO standard fire curve. However, to assure an appropriate base of comparison, the gas temperature measured at thermocouple 41 (compare red bordered sectional drawing ‘B-B’ in Figure 28) is chosen. Figure 29 shows the predicted temperature distribution in the section after 60 minutes exposure to this temperature set as computed with ABAQUS.

Whereas the insulation material is characterised by temperature gradient, the outer and inner stainless steel tube show nearly uniform cross-sectional temperatures.

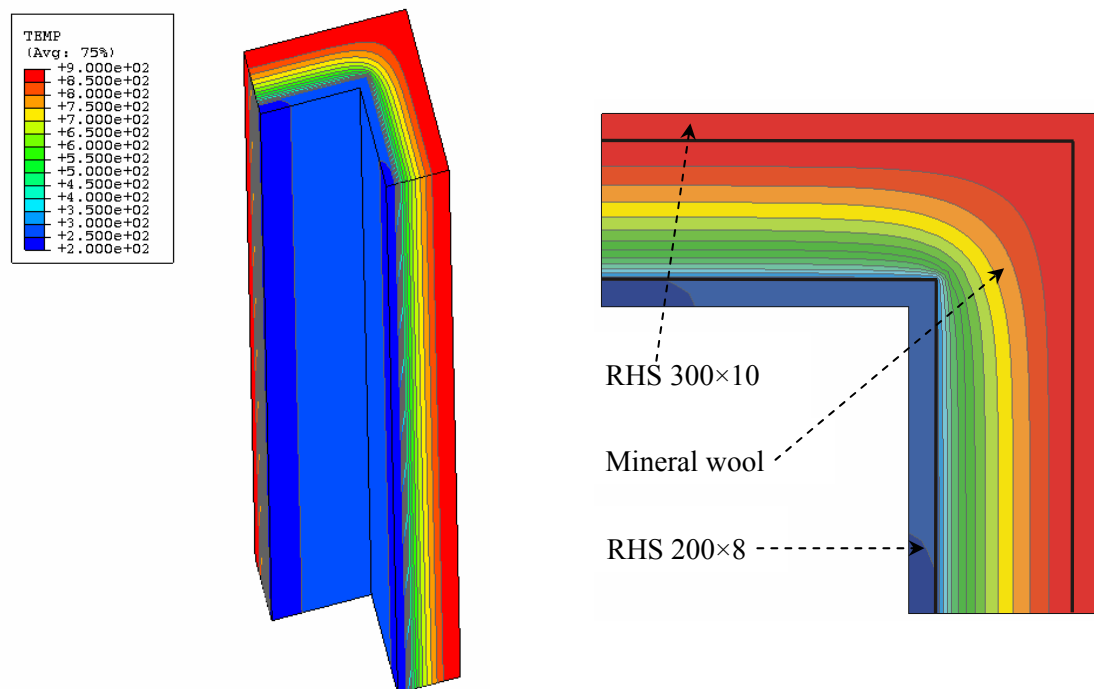


**Figure 29** Temperature distribution in nested tubes after 60 minutes exposure to furnace temperatures

Figure 30 exhibits the recorded cross-sectional column temperatures for the outer tube at thermocouples 2, 5, 8 and 11, which are located at test specimen centre (see Figure 28). The solution of the thermal problem with ABAQUS is presented for stainless steel material properties according to EN 1993-1-2 as well as Gardner. The analysis is based on the measured gas temperature at thermocouple 41. It is obvious that the recorded cross-sectional temperatures diverge. The difference can be explained by non-uniform heating in the fire test with temperature differences of almost 200°C within the outer cross RHS section. The cross-sectional temperatures computed with ABAQUS can be found at the lower limit of the recorded temperatures, where the solution based on the conventional EN 1993-1-2 material properties leads to higher temperatures than based on the revised values according to Gardner.

Concerning the inner tube, the comparison between numerical results and test data is illustrated in Figure 31. There is also a discrepancy between the cross-sectional temperatures measured at different thermocouples (14, 17, 20 and 23). The numerical temperatures computed with ABAQUS are once again lower than the recorded ones.

In conclusion it can be stated that stainless steel material properties according to EN 1993-1-2 as well as Gardner are appropriate to model the heating process. This is underlined by numerical results for the outer tube which are in good accordance with test data. However, numerical and test results diverge for the inner tube. This is due to missing material properties for mineral wool, which are estimated in the numerical model. It is clear that the alteration of thermal properties of insulation material has great influence on the cross-sectional temperature of the inner tube. However, these properties are not changed for following investigations. This is because the difference between recorded and computed temperatures is acceptable in view of the high scatter of recorded cross-sectional temperatures.

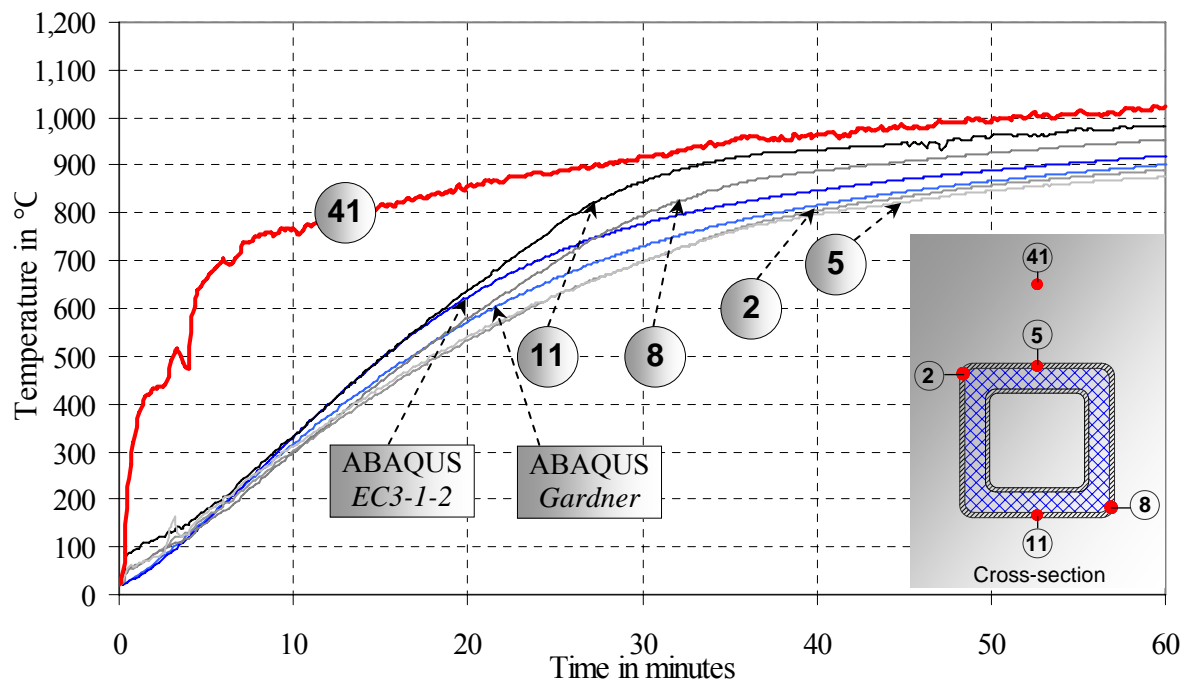


**Figure 30** Comparison between test data and numerical results for outer tube RHS 300×10

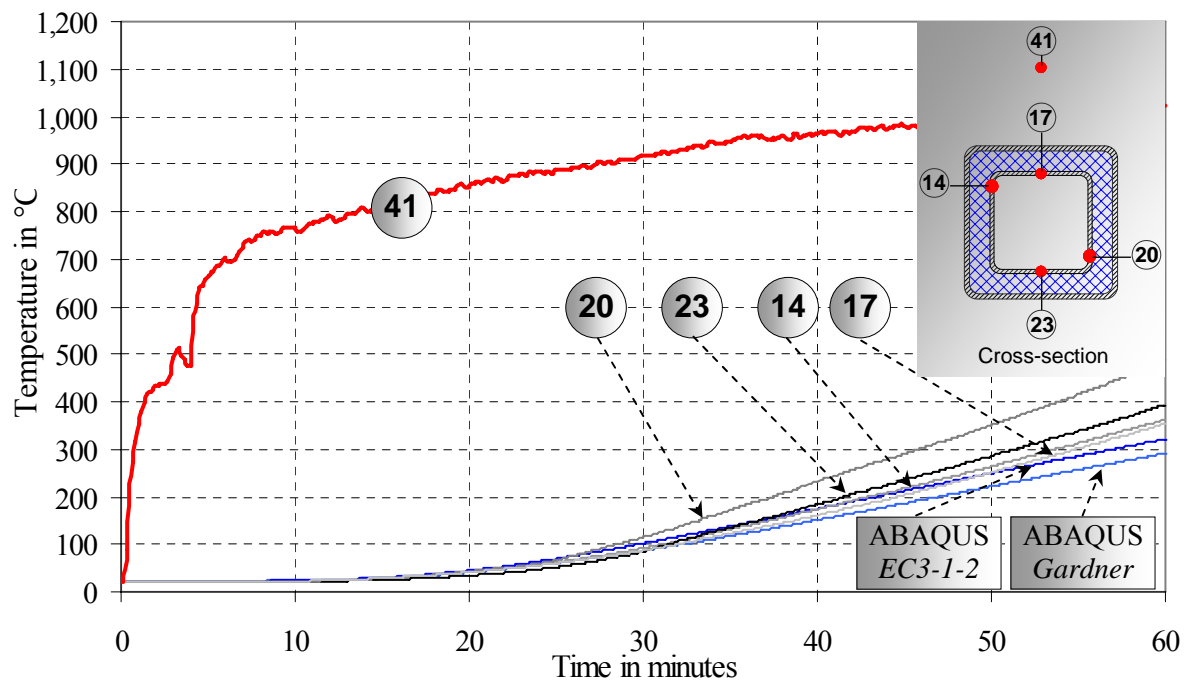


**Figure 31** Comparison between test data and numerical results for inner tube RHS 200×8



### Mechanical analysis

A mechanical analysis of the nested tubes cross-section is performed with the computer program BoFIRE. To simplify the model the outer tube is neglected, which can be justified by high cross-sectional temperatures after 30 and 60 minutes exposure to ISO standard fire (see Figure 30). This is because the high cross-sectional temperatures strength and stiffness degrade, which results in minor residual load-bearing capacity. At the example of the simplified model, the load-bearing behaviour of stainless steel at elevated temperatures is clarified. The comparison to identical columns out of S235 carbon steel shows the specific advantages of stainless steel.

The comparison of material properties (see section 3) indicates that the use of stainless steel is especially interesting for cross-sections heated to temperatures above 400°C. Thus, uniform cross-sectional temperatures are assumed in the following numerical analysis. This is justified by Figure 29. The computer program BoFIRE is used to calculate stainless steel columns with varying length from 2 to 12 m. Heated cross-sections with uniform temperatures ranging from 400 to 900°C are examined for each column length. The cross-section and static system of the investigated column are shown in Figure 32. An imperfection of  $L/300$  is assumed covering geometrical and structural imperfections. The ultimate load-bearing capacity is calculated by incrementally increasing the applied load of the heated cross-sections.

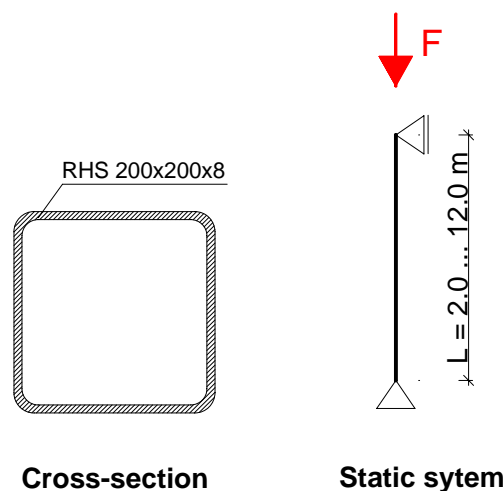


**Figure 32** Simplified cross-section and static system of the nested tubes

The outcome of the parametric study can be seen in Figure 33 for selected cross-sectional temperatures of 400°C, 600°C and 800°C. For cross-sectional temperatures of 400°C, the regarded stainless and carbon steel columns show almost the same load-bearing capacity. However, non-slender stainless steel columns with length less than 3 m show higher load-bearing capacity than carbon steel columns.

Considering the columns with cross-sectional temperature of 600°C, the superior material behaviour of stainless steel at higher temperatures becomes clear. This is underlined by much higher load-bearing capacity of the stainless steel columns in comparison to carbon steel columns, which results from the degradation of important material properties as elastic modulus and yield strength (compare Figures 1 and 2).



Further increased cross-sectional temperature of 800°C leads to minor residual load-bearing capacity of carbon steel. In contrast to this, the stainless steel columns show reasonable load-bearing capacity.

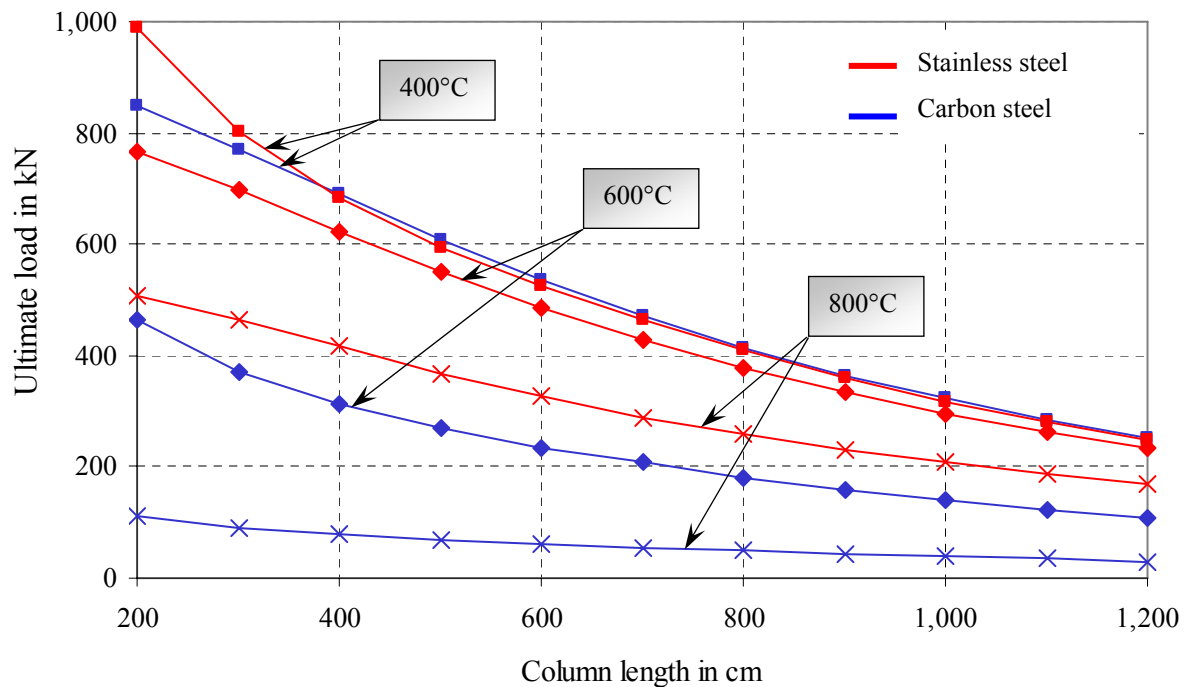


**Figure 33 Ultimate loads for varying column length and cross-sectional temperatures**

The investigated columns are once again presented in Figure 34 to underline the improved load-bearing behaviour of stainless steel at elevated temperatures. In this figure, all considered cross-sectional temperatures from 400°C to 800°C are presented. The ultimate load of stainless steel column is divided by the corresponding value for carbon steel columns.

As it can be seen, the ultimate loads for cross-sectional temperatures between 400°C and 500°C are very similar using both materials. Yet for temperatures above this point the advantageous material properties of stainless steel results in sharply increased ultimate loads in comparison to carbon steel. Taken the cross-sectional temperature of 600°C, this results in an ultimate load ratio of about 2.0. The corresponding ratio rises exceedingly with increasing cross-sectional temperatures of 700°C and 800°C.

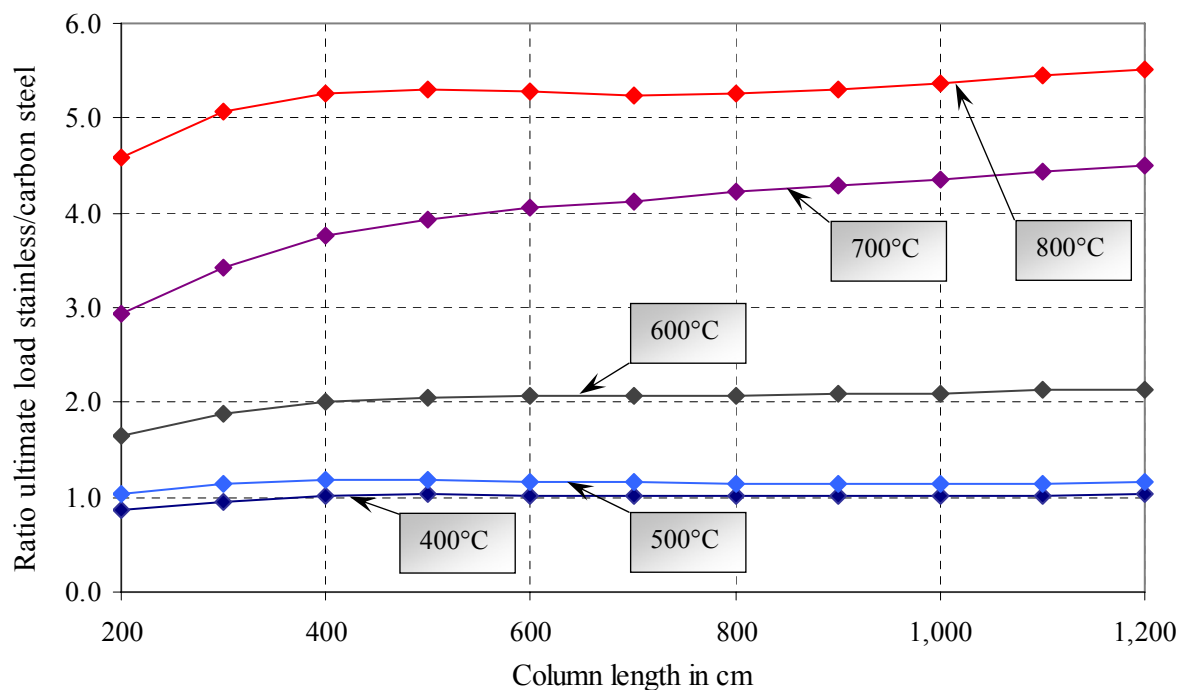


**Figure 34 Ratio ultimate loads of stainless and carbon steel column for varying column length and cross-sectional temperatures**

The aim of this work package is to develop building applications where structural stainless steel members can demonstrate fire resistance times of 30 or 60 minutes. Stainless steel shows superior load-bearing behaviour at high cross-sectional temperatures, in particular from 600°C to 800°C. This range corresponds to the resulting cross-sectional temperatures of an unprotected steel column subjected to 30 minutes ISO standard fire.

Hence it was examined if the cross-section could be further simplified by omitting the outer tube and insulation material. The unprotected stainless steel column was exposed to ISO standard fire in thermal analysis and once again computed using material properties of carbon steel.

As it can be seen in Figure 35, the stainless steel cross-section heated slower than the carbon steel cross-section. After 30 minutes exposure to the ISO standard fire, the temperature at the measure point (see cross-section in Figure 35) was 698°C for stainless steel in comparison to 740°C for carbon steel, which amounts to a temperature difference of 42°C. After 60 minutes, this difference amounts to 48°C with cross-sectional temperatures of 848°C and 896°C for stainless and carbon steel, respectively.

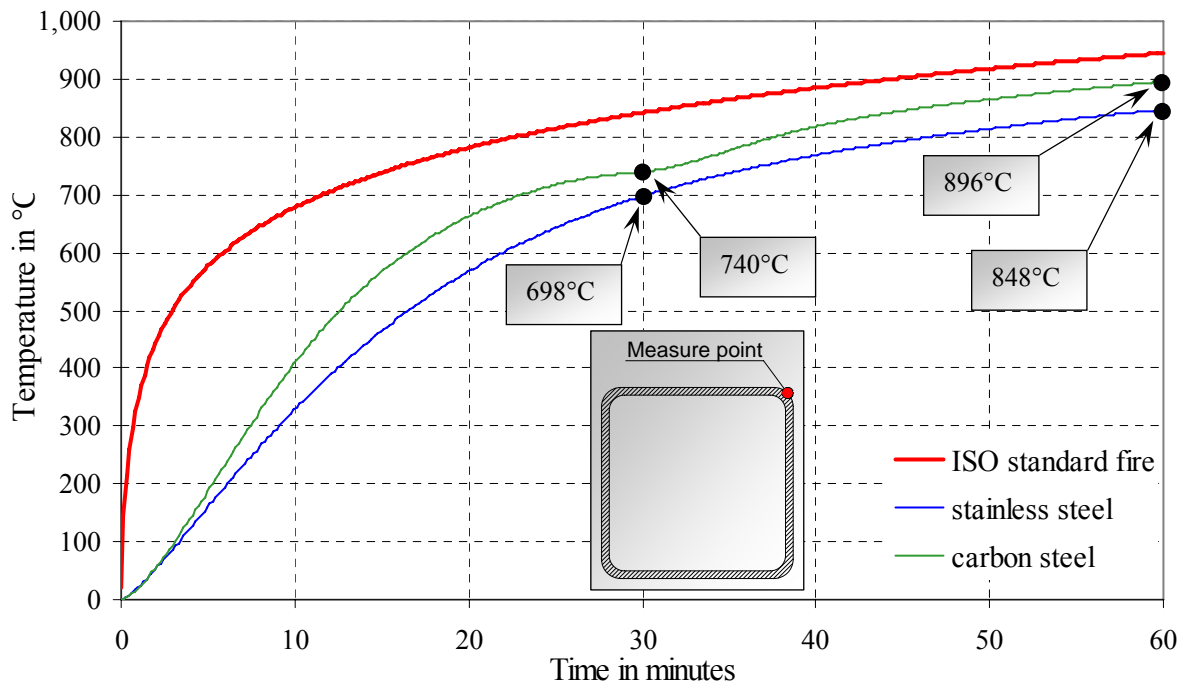
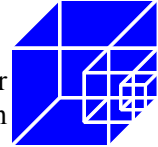


**Figure 35 Cross-sectional temperature for unprotected stainless and carbon steel column**

Stainless steel shows far better load-bearing behaviour for these high temperatures than carbon steel, which is also presented in [8].

A load-bearing analysis was carried out for the heated stainless and carbon steel column. An ultimate load of 691 kN was obtained for the stainless steel column corresponding to 54 % of its plastic resistance at ambient temperature. In contrast to this, the ultimate load of the carbon steel column was only 14 % of its plastic resistance.

Mechanical actions for structures in fire shall be combined for accidental design situations. In accordance with EN 1993-1-2 the reduction factor  $\eta_{fi}$  for load combination should be taken as:

$$\eta_{fi} = \frac{G_k + \psi_{fi} \times Q_{k,1}}{\gamma_G \times G_k + \gamma_Q \times Q_{k,1}}$$

with:

- $\eta_{fi}$  reduction factor;
- $G_k$  characteristic value of a permanent action;
- $Q_{k,1}$  characteristic value of the leading variable action;
- $\gamma_G$  partial factor for permanent actions;
- $\gamma_Q$  partial factor for variable action 1;
- $\psi_{fi}$  combination factor according to EN 1991-1-2.

Figure 36 exhibits the variation of the reduction factor depending on varying load ratio and three different combination factors  $\psi_{fi}$ . It should be noted that partial factors  $\gamma_G = 1.35$  and  $\gamma_Q = 1.5$  were assumed.

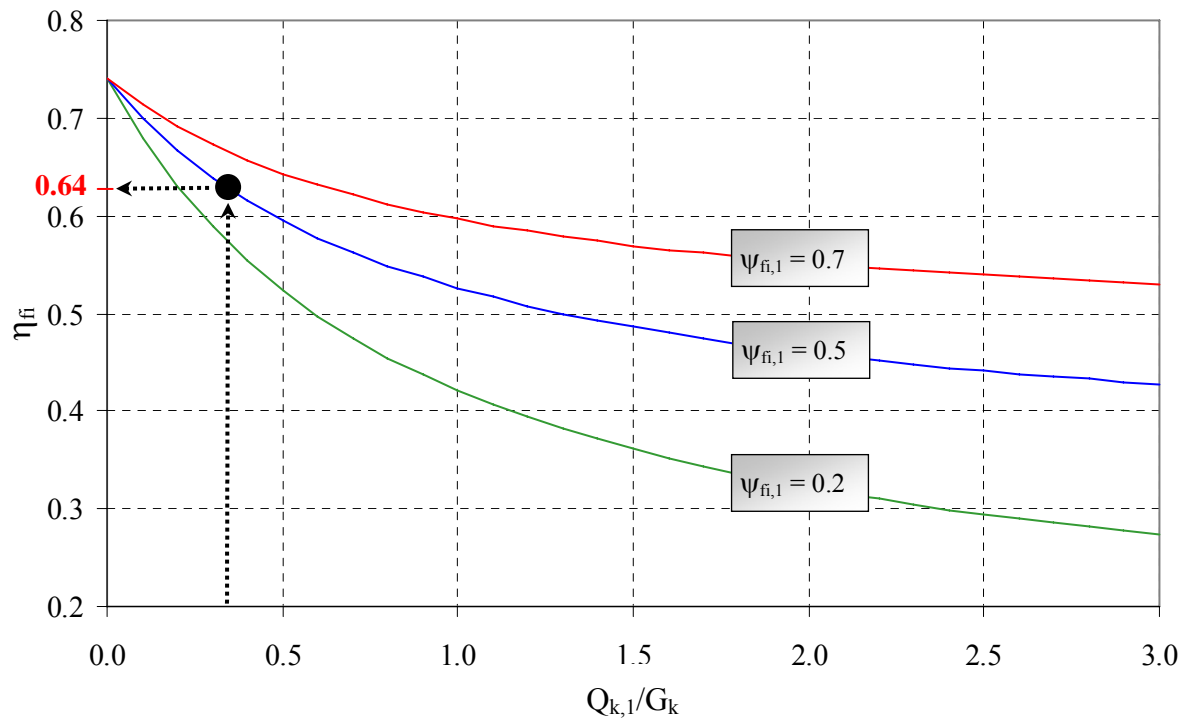


**Figure 36** Variation of the reduction factor  $\eta_{fi}$  depending on varying load ratio  $Q_{k,1}/G_k$

If for instance a ratio of  $Q_{k,1}/G_k = 0.3$  with partial factor  $\psi_{fi,1} = 0.5$  is assumed the reduction factor results to  $\eta_{fi} = 0.64$ . This means that the ultimate load of the stainless steel column corresponds to load ratio of 84 % in comparison to 22 % for the carbon steel column. It is obvious that the second load ratio is not economical.





## 5.4.2 Column in SIPOREX wall

### Introduction

In the second analysed load-bearing structure an unprotected stainless steel column was integrated in a SIPOREX wall as presented in Figure 37. The column was hence exposed to fire from one side. A rectangular cross-section RHS 200×100×6 mm was chosen in accordance with VTT.

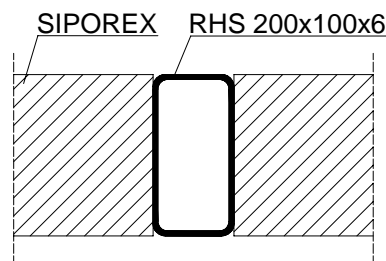


**Figure 37** Cross-section of column in SIPOREX wall

The column had a length of 3 m with different end conditions. In the first case, hinged end-conditions were investigated to account for fire in a compartment. Fixed end conditions were considered subsequently, which simulates the behaviour of columns passing through several storeys with fire in only one compartment. In this case, relative stiffness of the column in the protected compartments resembles constraint of the column exposed to fire. An example for the latter case can be found in Figure 38.

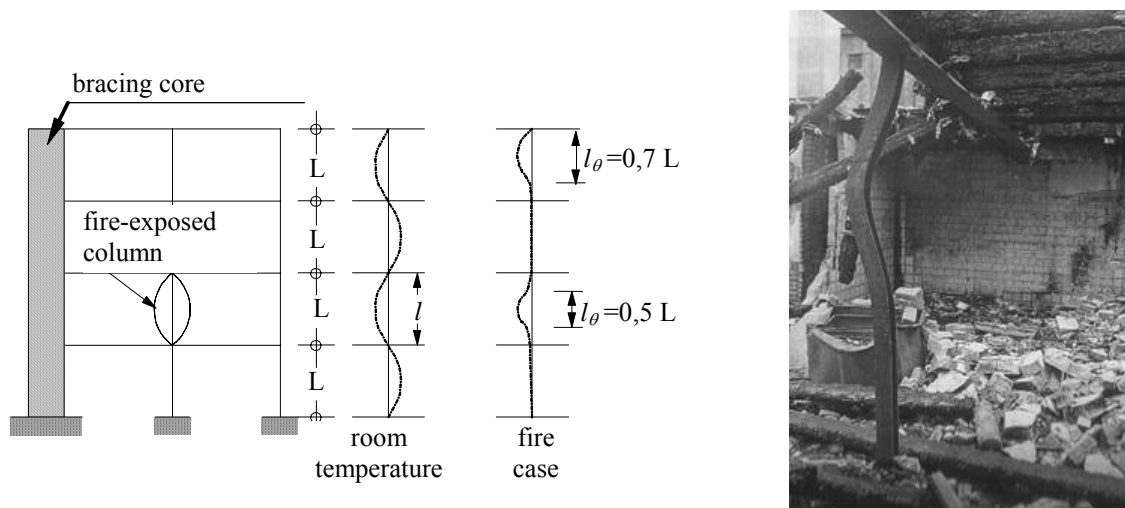


**Figure 38** Buckling length at elevated temperatures (left) and example of fixed end conditions (right)

### Thermal analysis

A two-dimensional analysis was carried out to establish the temperature distribution for exposure to ISO standard fire up to 60 minutes. The diffusive heat transfer element DC2D4 was chosen, which is a four node linear heat transfer element. The elements had consistent size of 3 mm.



Thermal properties of the wall material SIPOREX were taken as defined by VTT as temperature-independent values:

- Thermal conductivity:  $\lambda = 0.12 \text{ W/(m}\times\text{K)}$
- Specific heat capacity:  $c_p = 1,000 \text{ J/(kg}\times\text{K)}$
- Emissivity:  $\varepsilon = 0.7$
- Density:  $\rho = 500 \text{ kg/m}^3$

The heating of stainless and carbon steel was computed using the thermal properties according to Gardner and EN 1993-1-2, respectively. Heat transfer included both radiation and convection. **Cavity radiation within the hollow section is neglected. The outcome is lower temperatures for the unexposed parts than could be expected from real fire exposure. This might result in overestimation of strength and stiffness of the unexposed parts. On the other hand, the assumption results in increased calculated thermal bowing of the column. These contrary effects are supposed to cancel out each other. As these investigations are qualitative and not quantitative, this assumption can be justified.** Figure 39 shows the heated SIPOREX cross-section with integrated stainless steel column at 30 and 60 minutes exposure to ISO standard fire.

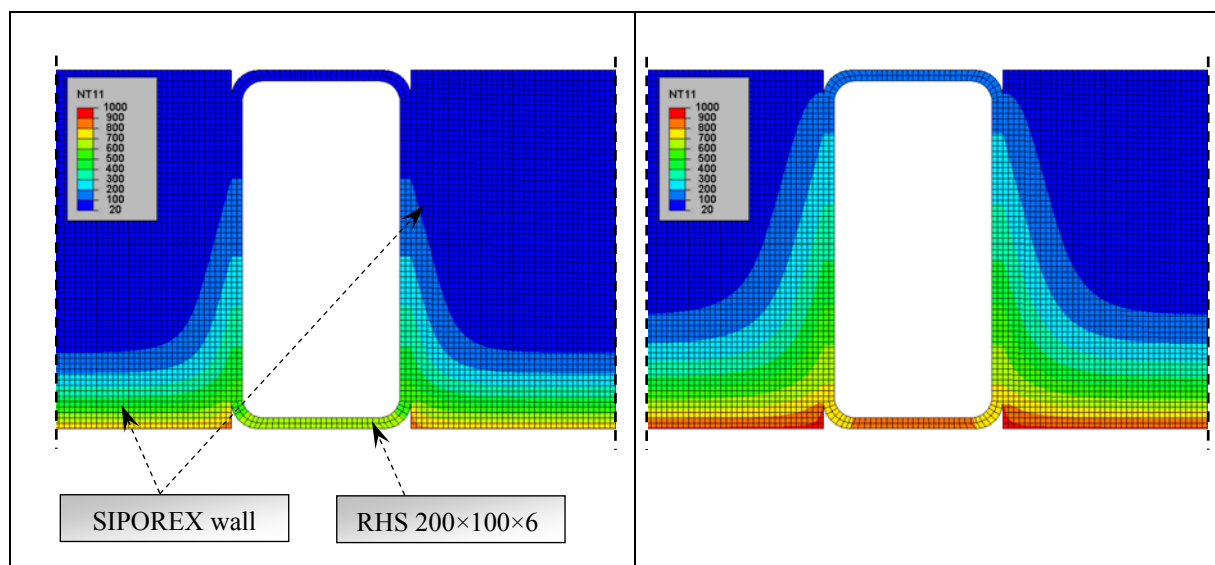


**Figure 39 Heated cross-section after 30 minutes (left) and 60 minutes (right) exposure to ISO standard fire**

As it can be seen from this figure, the SIPOREX wall is efficient in isolating the integrated stainless steel column. After 30 minutes of exposure to ISO standard fire, only approximately half of the cross-section was affected by elevated temperatures. After 60 minutes the whole cross-section was heated. However, there is a great discrepancy between the fire-exposed and unexposed cross-sectional parts with maximum temperature difference of almost 600°C.

For the following mechanical analysis of the heated column results from the two-dimensional thermal analysis were transferred to the three-dimensional mechanical model. Therefore the cross-section was divided into twelve areas (see Figure 40) characterised by nearly constant temperature distribution. The cross-sectional temperature for each area at a certain time was given by amplitude, which were implemented in the mechanical model. For each area the highest temperature was stored, which is a conservative approach.



The cross-sectional temperature development for both stainless and carbon steel is also presented in Figure 40 for selected areas 1, 5, 10 and 12. It is obvious that carbon steel heats faster than stainless steel. Moreover, the temperature difference increases for unexposed parts of the column. Whereas the difference after 60 minutes is about 50°C for regions 1 and 5, it already amounts to approximately 120°C and 180°C for regions 10 and 12, respectively.

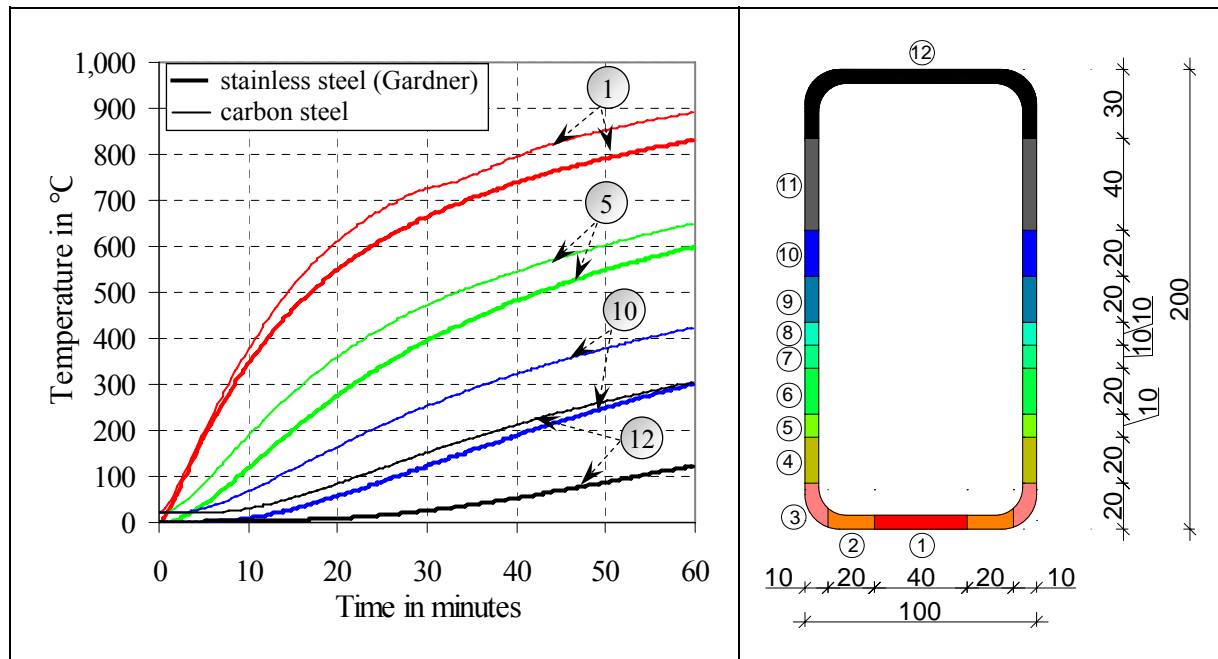


**Figure 40** Selected cross-sectional temperature development of column in SIPOREX wall (left) and definition of cross-sectional areas (right)

In addition, the calculated temperature distribution was compared to test results from fire tests performed by VTT. The comparison included three measure points at the stainless steel column: At the fire-exposed side of the cross-section (designated as ‘Measure point 1’ in Figure 41), at the cross-section centre (‘Measure point 2’) and at the fire-protected side (‘Measure point 3’). For each measure point, results from numerical analysis using both stainless steel material properties according to Gardner and EN 1993-1-2 were compared to available test data. It should be noted that the thermocouples in the test were arranged at different column heights.

In general, it can be seen once again in Figure 41 that revised material properties according to Gardner result in slower heating of the cross-section. Regarding measure point 1, it is obvious that calculated temperatures overestimate measured temperatures at thermocouples TC1 and TC9 to some extent. However, accordance between test and numerical results can be seen as acceptable, especially when using Gardner’s revised material properties.

The second measure point at the mid of the cross-section is characterised by higher scatter of recorded temperatures at thermocouples TC7, TC18 and TC27. For instance, the difference between temperatures recorded at TC18 and TC7 amounts to approximately 160°C after 60 minutes exposure to ISO standard fire. In view of this high discrepancy, it is difficult to assess the quality of numerical results, which are close to values of thermocouple TC27.

The last measure point is arranged at the unexposed side of the column. In contrast to the previous regarded point, recorded temperatures diverge slightly. However, numerical simulation



with ABAQUS predicted far slower heating at this point. The maximum difference between measured and computed temperatures is 150°C after 60 minutes.

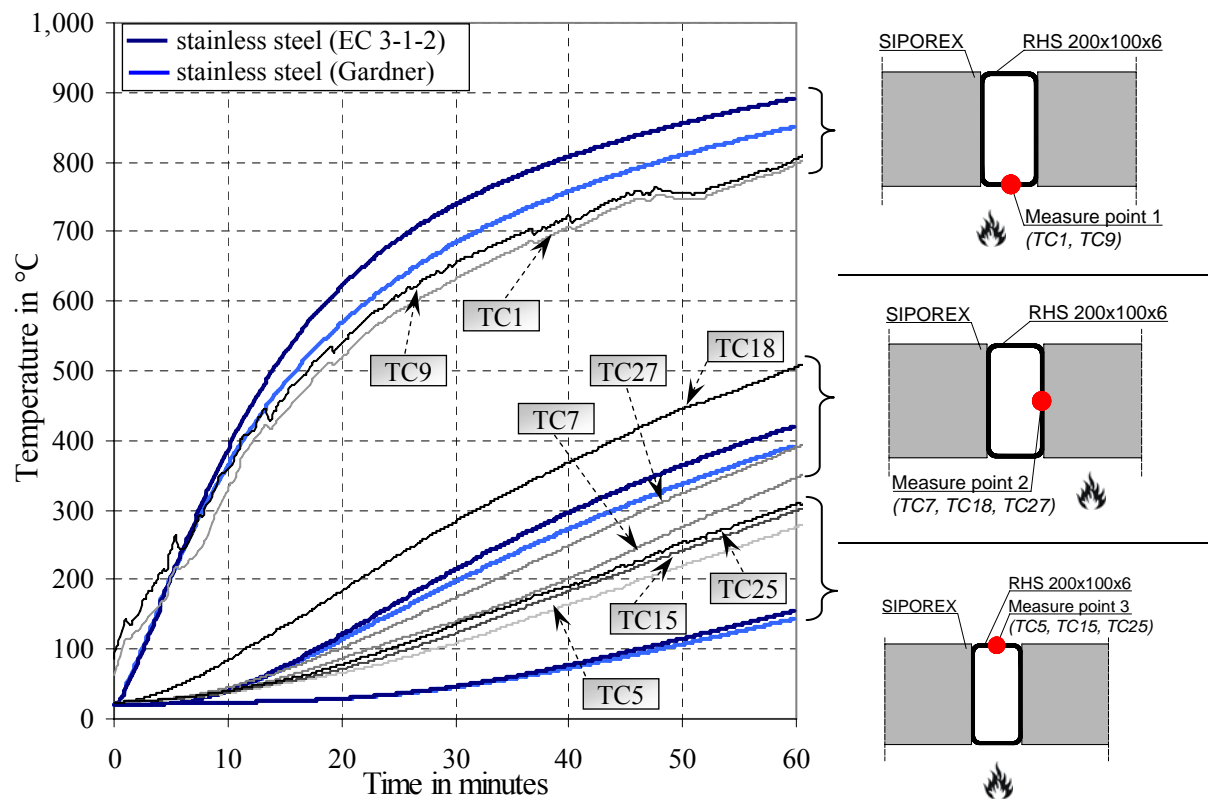


**Figure 41** Comparison of recorded and calculated cross-sectional temperatures

### Mechanical analysis

Fire tests performed by VTT were restricted to unloaded stainless steel specimens. These investigations are hence extended by numerical analysis with ABAQUS to establish the load-bearing behaviour of stainless steel structures at elevated temperatures.

### Elements

Dimensions of the selected column advise modelling with shell elements. The library of ABAQUS offers various shell elements. In accordance with investigations carried out in [9], the general-purpose conventional shell element S4R with six degrees of freedom per node is chosen (see Figure 42). This element provides robust and accurate solutions to most applications. It switches automatically between thin shell theory, which means that the Kirchhoff constraint must be fulfilled (i.e. the shell normal remains orthogonal to the shell reference surface), and thick shell theory taking the transverse shear flexibility into account.

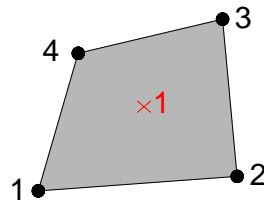


**Figure 42 Four-node reduced integration shell element S4R**

Moreover, it is characterised by reduced integration with hourglass control. The advantage of reduced integration is enhanced computational efficiency. The disadvantage to this method is the need to control the arising zero energy modes, the so-called hourglassing, that cause no straining at the integration points. As the zero energy modes starts propagating through the mesh, inaccurate results are obtained. Linear reduced-integration elements are in particular prone to this phenomenon, which is illustrated in Figure 43 at the example of an element subjected to bending moment  $M$ . It can be seen that fully integrated elements are capable of simulating the deformation, which is indicated by changed length of the dotted visualization lines and changed angle  $\alpha$ . Contrary to this, the element with reduced integration suffers from hourglassing, indicated by unchanged visualization lines and angle  $\alpha$ . The outcome is a zero-energy mode where the element has no stiffness and no strain energy is generated by the element distortion. It is obvious that elements suffering from hourglassing are unable to produce reasonable results.

Element with bending moment	Numerical approach	
	Full integration	Reduced integration
Deformation		

**Figure 43 Hourglassing of linear reduced-integration elements**

ABAQUS adds a small artificial stiffness to the elements in order to limit the propagation of hourglass modes and the appendant excessive deformations. In combination with a fine mesh, this hourglassing control is very efficient.



### Boundary conditions

The analysis was divided into two general steps. At first, a buckling analysis was conducted to generate both local and global imperfection modes. These imperfections were included in the subsequently carried out non-linear load-displacement analysis, where the ultimate load, and failure modes were determined.

Two different sets of boundary conditions were used, which are presented in Figure 44. As the column is integrated into the SIPOREX wall, rotation about the minor axis was excluded in both sets of boundary conditions. For that reason constraint equations were used to ensure that there were no end rotations about the non-buckling axis. In the first set, the lower support of the column was fixed against all degrees of freedom except for rotation about the major axis. In comparison to this, the upper end also allowed for vertical displacement in the direction of the applied load. With respect to the second set, all degrees of freedom were fixed with exception of vertical displacement of the upper support to allow for load introduction.

Referring to Figure 38, the two different boundary sets resemble columns in buildings that are subject to fire. Hinged-end conditions cover for example columns in one-storey building. Contrary to this, in multi-storey buildings with passing through columns fixed end-conditions can be obtained provided that only one storey is exposed to fire and that the different storeys are separated from each other by appropriate fire protection means.

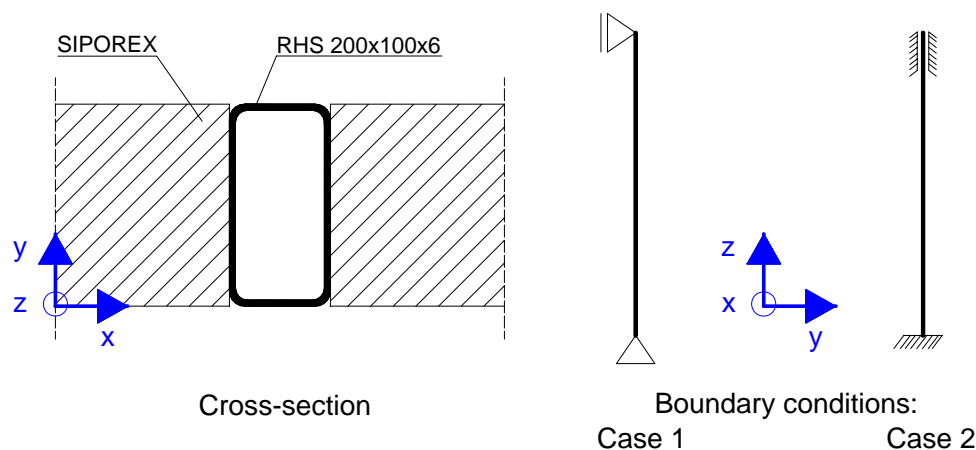


**Figure 44** Cross-section and sets of boundary conditions for column in SIPOREX wall

The aim of the investigations was to establish the general load-bearing behaviour of stainless steel columns so that the effects of bearings on ultimate load capacity, such as different head plates, could be excluded. As the column was modelled with shell elements, the boundary conditions of a beam had to be transferred to a folded plate model [10]. The ideal support of a beam is represented by a point, which can be incorporated in the model by applying a rigid body constraint. This is a collection of nodes ('tied nodes'), whose motion is governed by the motion of a single node (the so-called 'reference node'). The relative positions of the nodes and elements that are part of this constraint remain constant throughout a simulation. Hence the constituent elements do not deform but can undergo large rigid body motions. Loads are introduced through the reference point of the constrained node set.

Rigid bodies are recommended to model relatively stiff parts of a model, which is true for head plates. The advantage of simplifying the numerical model is associated with computa-



tional efficiency of this approach. The reference point and its appendant nodes are presented in Figure 45 at the example of the upper support.

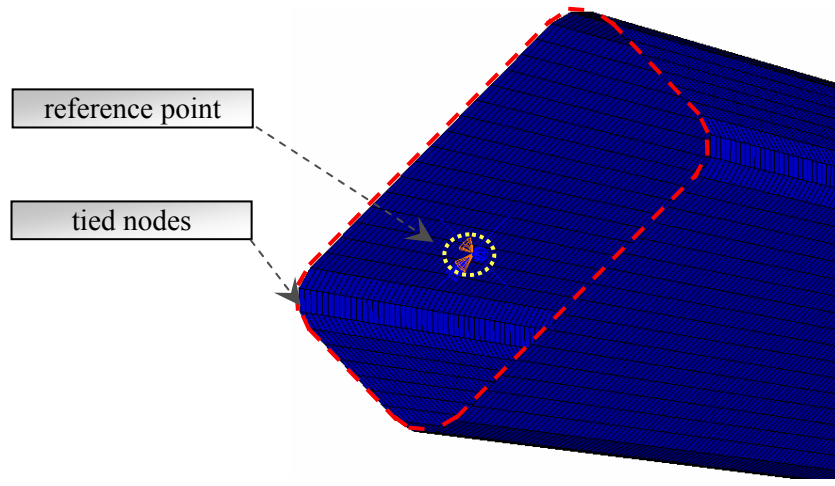


**Figure 45** Numerical modelling of supports of the column in SIPOREX wall

### Buckling analysis

Linear elastic eigenmode simulations were conducted to take the effects of local and global imperfections into consideration in the Finite Element model. Figure 46 exhibits the assumed global and local imperfection. The deformed mesh coordinates were stored and their superposition was assumed as final imperfection pattern for the following mechanical analysis of the heated columns, where the global imperfection is scaled to  $L/500 = 6$  mm and the local imperfection to 1 mm.

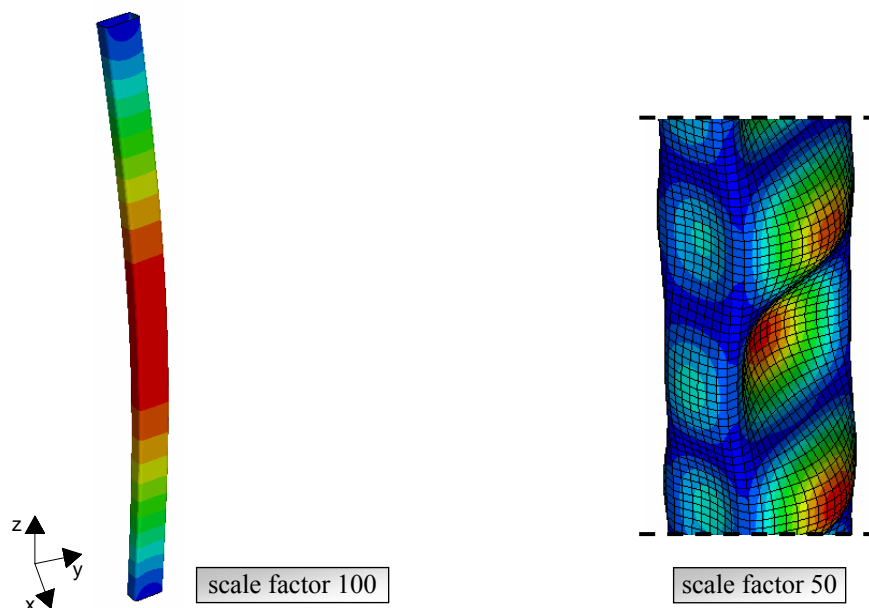


**Figure 46** Applied global (left) and local (right) imperfections





### Load-displacement non-linear analysis

Finally, non-linear load-displacement analysis of the heated stainless steel column was performed, where the previously established imperfection pattern was used as initial condition. A vertical load of 359 kN, which corresponds to load ratio of 50 % at room temperature, was applied with an eccentricity of 20 mm at the upper reference point of the stainless steel column. The column was subsequently heated for 60 minutes according to the cross-sectional temperature amplitudes obtained from the formerly performed thermal analysis. If the column still had load-bearing capacity after having been heated up, the load would be increased into the last step until failure occurs.

At first, hinged end conditions according to Figure 44, case 1 were considered. As it can be seen from Figure 47, the stainless steel column failed by flexural buckling. Local buckling of the column is presented at the right side of the same figure.

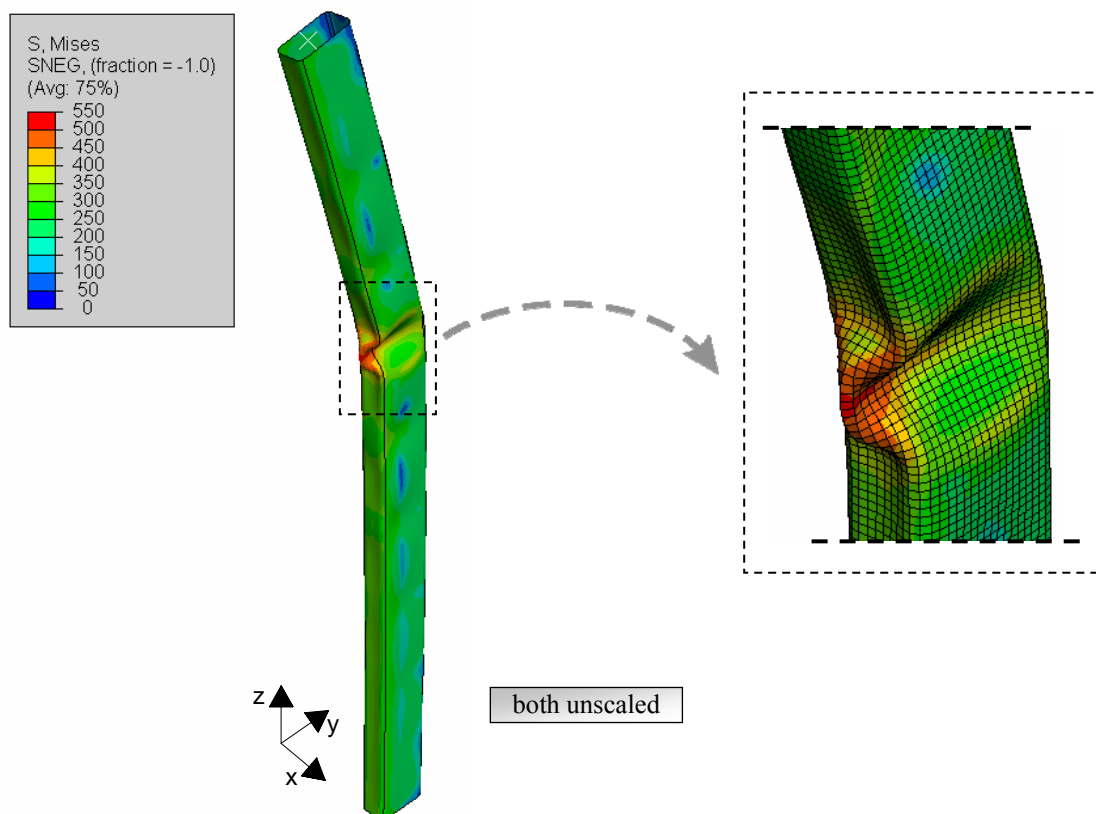
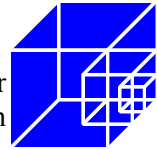


**Figure 47** Deformed pin-ended stainless steel column (left) and detail of local buckling (right) after 13 minutes

Figure 48 shows the horizontal displacement  $u$  at the centre of the column as well as the cross-sectional temperature at area 1 against time. It is obvious that the displacement was only about 40 mm for temperatures of 400°C at area 1. However, the displacement increased exceedingly for higher cross-sectional temperatures. Thus, the column failed after approximately 14 minutes due to greater bending moments.

The simulation was once more performed using the material properties of carbon steel with yield strength of 235 MPa. This column achieved fire resistance of 30 minutes. Figure 49 compares the deformations of both columns against cross-sectional temperature. In contrast to





the stainless steel column this column did not fail by overall flexural but local buckling. Thus, maximum horizontal deformations were less than 10 mm in comparison to almost 520 mm for the stainless steel column.

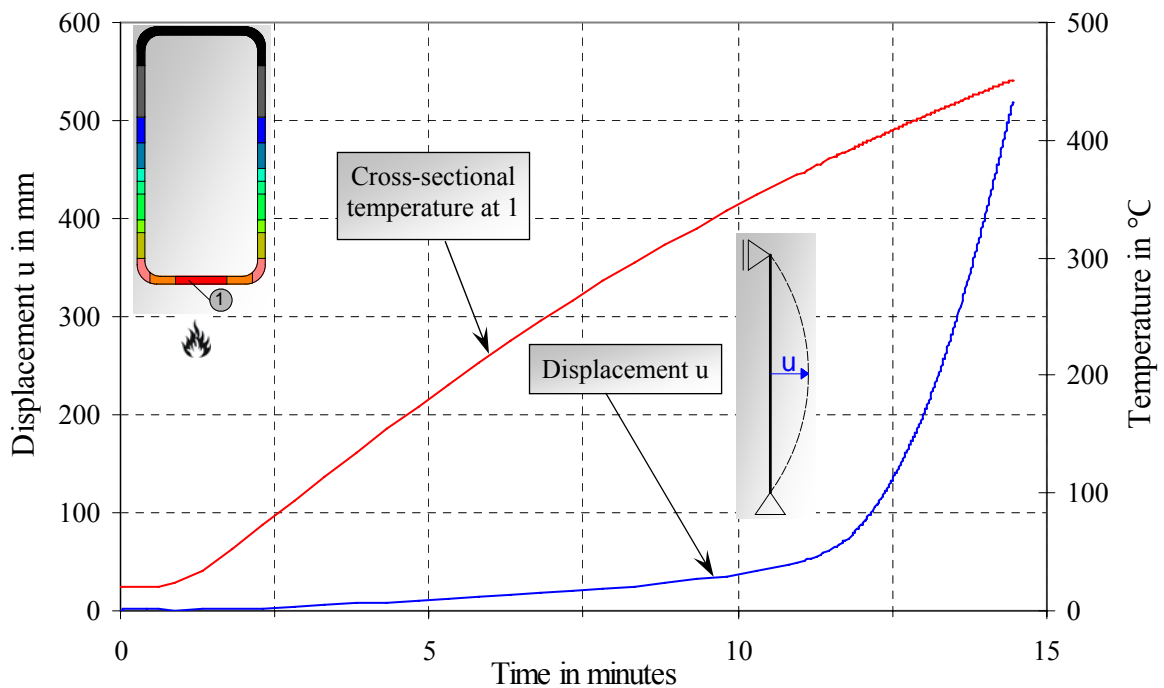


**Figure 48** Results from load-bearing analysis of pin-ended stainless steel column integrated in SIPOREX wall

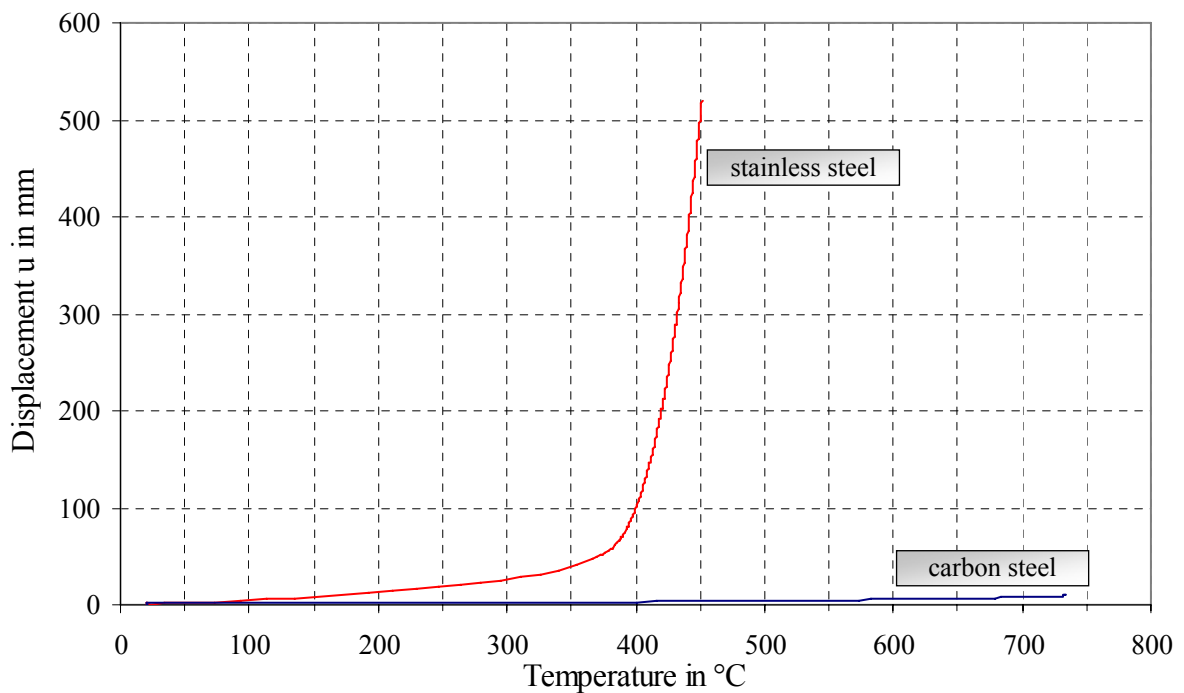




**Figure 49 Comparison of horizontal deformations at column centre against cross-sectional temperature**

The different failure modes result from the varying stress-strain relationship of carbon and stainless steel at elevated temperatures. Columns are mainly used as compression members, which are characterised by small strains. This stands in contrast to load-bearing structures such as beams, which are subject to flexural loads. As illustrated in Figure 50, logarithmic strains were for both columns comparatively low. The ultimate strain for the stainless steel column was approximately 1 %, whereas the carbon steel column failed with an ultimate strain exceeding 3 %.

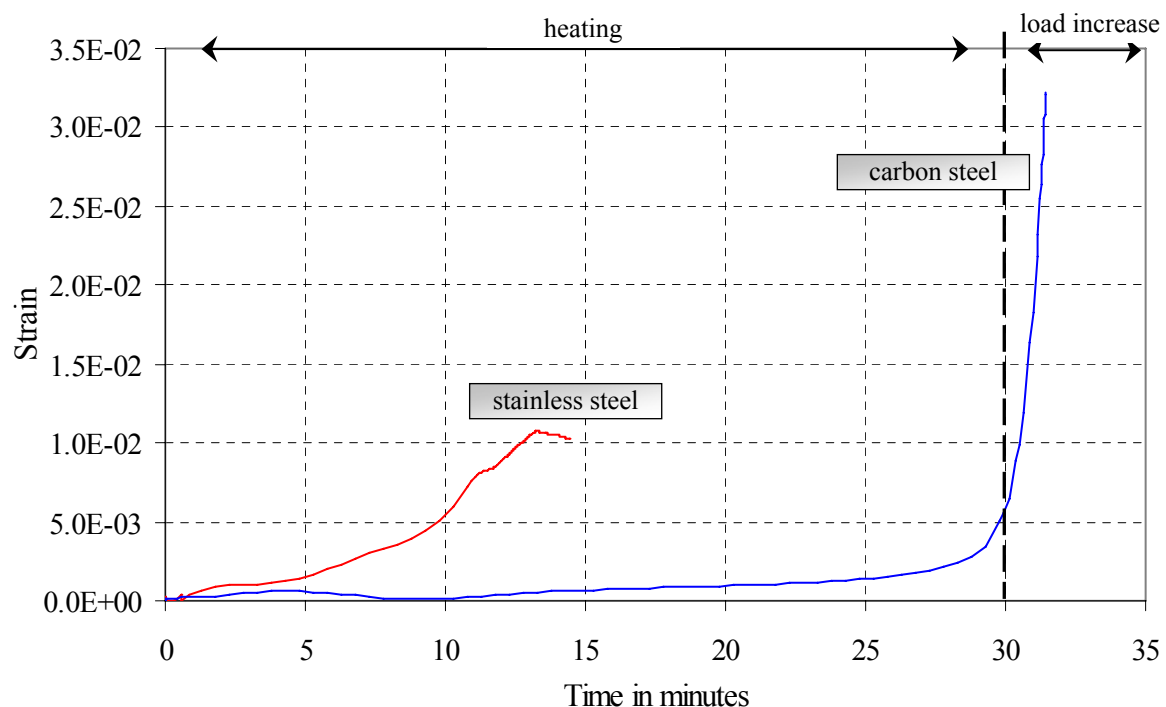


**Figure 50 Comparison of logarithmic strains for pin-ended column**

Figure 51 compares the stress-strain relationships of stainless and carbon steel for selected elevated temperatures and strains less than 5 %. The complete stress-strain relationship can be found in Figure 3. It is obvious that yield strength of stainless steel is higher than of carbon steel for large strains, i.e. strains exceeding values of 5 %.

However, for small strains carbon steel tends to be far stiffer than stainless steel. As presented in Figure 51, this is true for temperatures less than 500°C. Both columns were protected by the surrounding SIPOREX wall. Therefore few cross-sectional parts were heated to temperatures higher than 500°C after 30 minutes of ISO standard fire, which is presented in Figure 39 and Figure 40. Only the fire-exposed side of the rectangular steel profile and its adjacent fillets were heated to such high temperatures.

This explains the different failure modes. Stiffness of the stainless steel column was reduced to a great extent in comparison to the carbon steel column. Therefore the column experienced large deformations resulting in additional loads according to the second-order theory. In contrast to this, the carbon steel column failed by local buckling of fire-exposed side. This is the outcome of sharply reduced yield strength at temperatures about 700°C (see Figure 1).

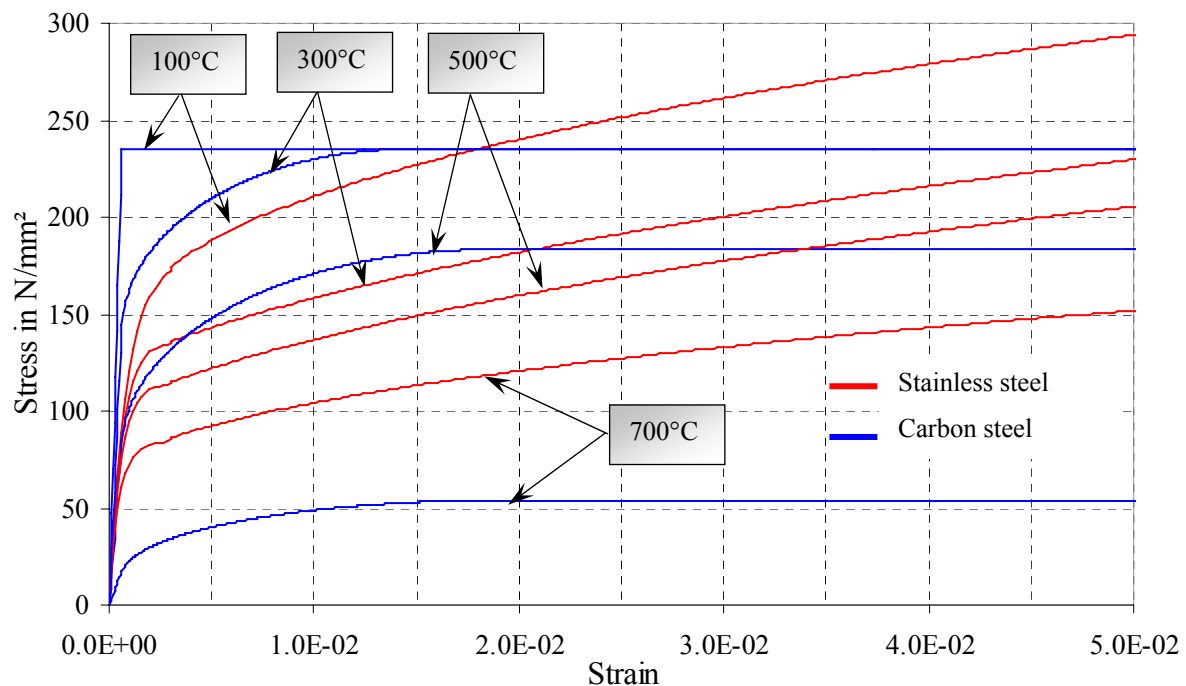


**Figure 51 Comparison of stress-strain relationship at elevated temperatures**

In order to achieve R30 classification of the stainless steel column, case 2 (see Figure 44) with fixed boundary conditions was regarded. Figure 52 compares the displacement of both columns at the column centre. In contrast to the pin-ended column, large horizontal displacements were prevented so that both columns failed by local buckling. In general, the stainless steel column deformed less than the carbon steel column.

Concerning the stainless steel column, the successive load increase finished with an ultimate load of 368 kN after 60 minutes of exposure to ISO standard fire. This corresponds to load ratio of approximately 51 % at room temperature. The deformed stainless steel column can be found in Figure 53. In contrast to this, the carbon steel column already failed after 33 minutes. Hence it only met the requirements for 30 minutes fire resistance.

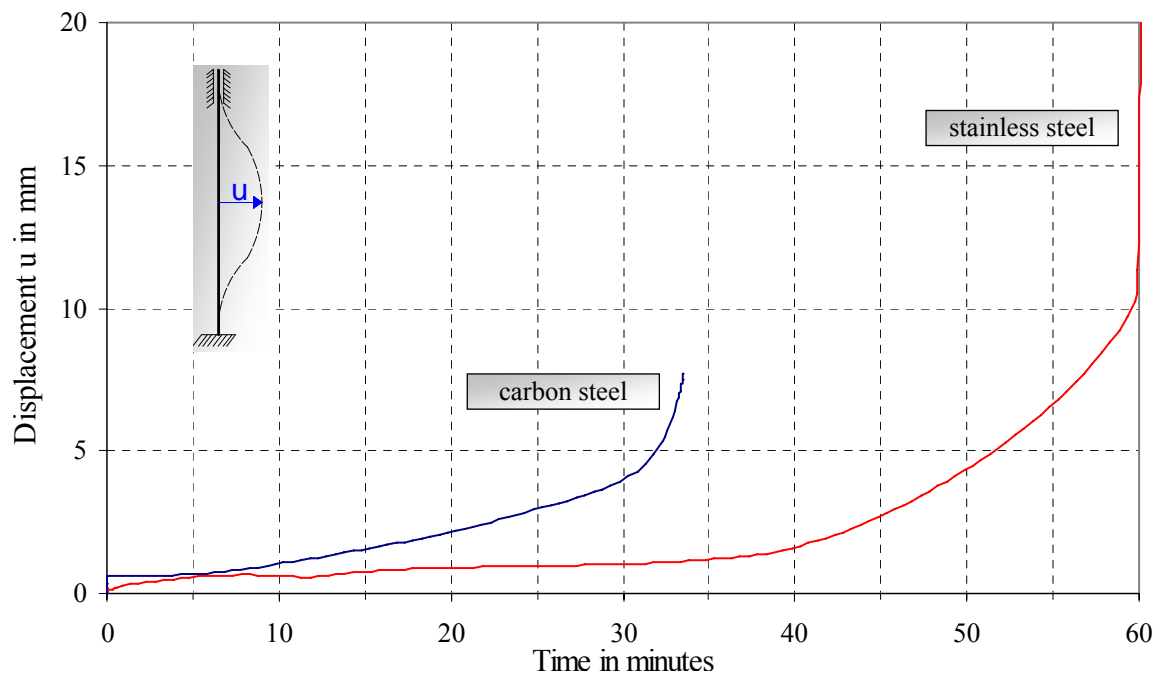


**Figure 52** Comparison of horizontal displacement at column centre against temperature

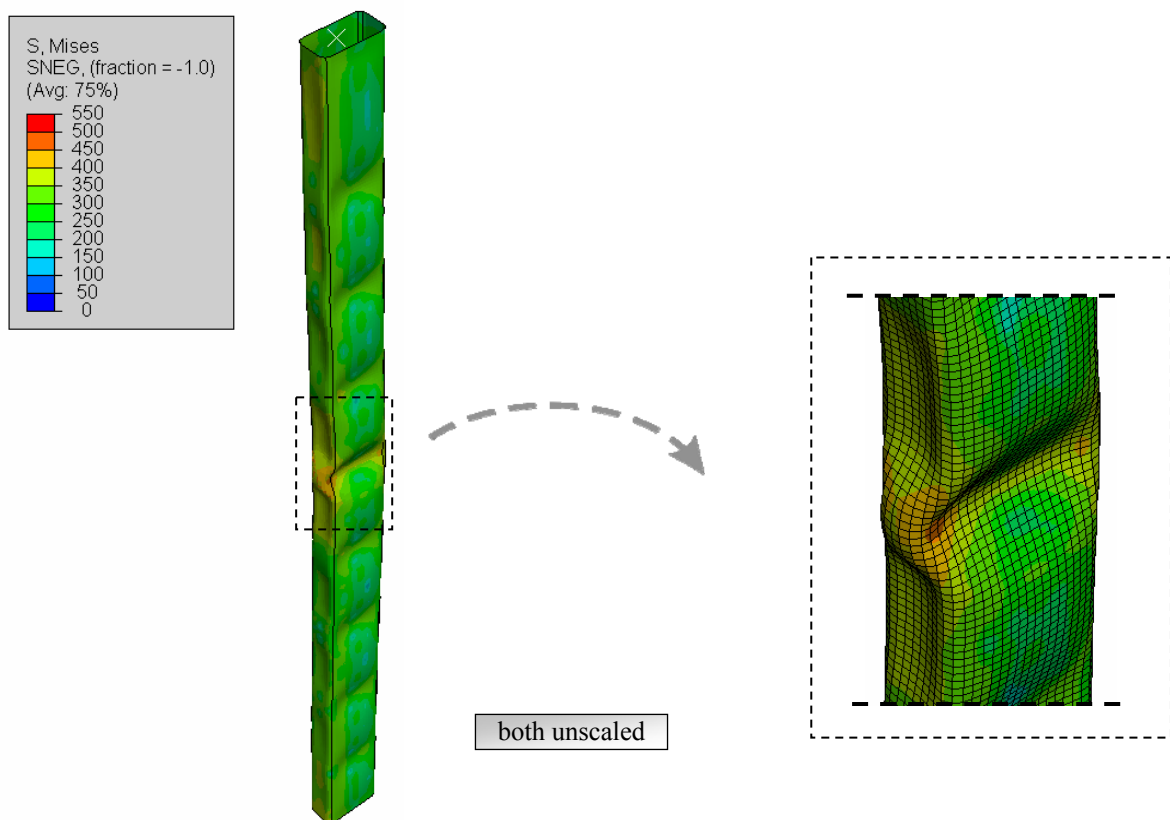
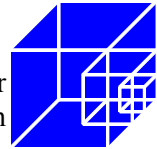


**Figure 53** Deformed stainless steel column (left) with fixed end conditions and detail of local buckling (right) after 60 minutes



## 6 Development of design guidance

From the previous numerical investigations, reasonable scope of application for stainless steel in separating members and load-bearing structures was identified. Accordingly, its use is in particular interesting for cross-sectional temperatures between 600°C and 800°C. This is because for lower temperatures structural advantages over carbon steel are not distinct enough to justify far higher initial costs of stainless steel. Cross-sectional temperatures above 800°C result in sharp reduction of strength and stiffness. This means that fire safety requirements for 30 or 60 minutes can only be met for low load ratios, which is not economical.

There are different possibilities to attain the temperature range of 600°C to 800°C. Provided that the structure is exposed to ISO standard fire, temperatures in this range result after 30 minutes for unprotected stainless steel members. It was demonstrated that such members can achieve R30 classification with economic load ratios. This stands in sharp contrast to similar carbon members that only fulfil this classification at very low load ratio. Design aids for the particular target range of critical temperatures should be developed.

It is also feasible to protect structures partially. Only the fire-exposed parts are hence subject to high temperatures in the interesting range. As presented at the example of the stainless steel column surrounded by SIPOREX wall R60 classification is achievable. However, large deflections must be avoided by appropriate boundary conditions. This allows for large strains that are necessary to develop full yield strength of stainless steel.

Full protection of stainless steel is not recommended from economical and aesthetic point of view.



## **7 Conclusions**

### **7.1 Separating structures**

A new type of laser-welded stainless steel slab panel with rock wool insulation, developed by Kenno Tech Ltd., was investigated as example for separating structures.

It was shown in numerical investigations as well as in small scale fire tests that the insulation criterion I60 of EN 1993-1-2 for separating members can be realized. From the numerical investigation on the load-bearing behaviour an ultimate live load could be estimated for  $p \approx 750 - 800 \text{ kg/m}^2$ . According to the Eurocodes this complies with a load ratio of  $\mu_0 = 0.35$  at the fire situation.

Moreover, the results of the calculation at elevated temperatures demonstrated that the requested fire resistance of 60 minutes for load-bearing capacity was reached and failure did not occur.

### **7.2 Load-bearing structures**

Stainless steel offers many advantages over carbon steel, such as high corrosion resistance, low maintenance and aesthetics. As stainless steel is often chosen for the last reason, emphasis of the previous investigation laid on cross-sections where stainless steel is visible. These are unprotected as well as partially protected stainless steel columns.

The load-bearing behaviour of stainless steel clearly outperforms that of carbon steel at cross-sectional temperatures between 600°C and 800°C. This is in as far beneficial as these temperatures result from exposure to 30 minutes of ISO standard fire. The use of stainless steel is hence in particular interesting for load-bearing structures subjected to high temperatures. Thus, it is possible to achieve fire resistance times of 30 minutes for unprotected stainless steel columns. This stands in contrast to similar carbon steel columns, where this fire resistance time can only be accomplished with uneconomic load ratios or additional fire protection. The latter fact helps to reduce the difference between prices of stainless and carbon steel and hence justifies its use also from structural point of view.

Partial protection offers an option to benefit from the distinctive advantages of stainless steel at high cross-sectional temperatures. As demonstrated at the example of a stainless steel column integrated in a SIPOREX wall, fire resistance times of 60 minutes are achievable without further fire protection. Therefore large deflections should be avoided by means of appropriate end conditions. In this way, superior material costs of stainless steel as compared to carbon steel can be partly compensated as protection material can be omitted to achieve same fire resistance.

## **8 Recommendations for further work**

Further investigations are recommended to reduce the high deformations of the new developed KennoTech slab panel. Moreover, the load-bearing behaviour of stainless steel exposed to natural fires should be examined.

On the basis of gained knowledge of this research project, design aids should be developed to benefit from the optimal target range of critical failure temperatures of stainless steel.



## 9 References

### Codes

- 1 *European Committee for Standardization (CEN)*, prEN 1991-1-2: Eurocode 1: Actions on structures - Part 1-2: General actions - Actions on structures exposed to fire. Brussels: CEN 2002.
- 2 *European Committee for Standardization (CEN)*, prEN 1993-1-2: Eurocode 3: Design of steel structures - Part 1-2: General rules - Structural fire design. Brussels: CEN 2005.
- 3 *European Committee for Standardization (CEN)*, prEN 1993-1-4: Eurocode 3: Design of steel structures - Part 1-4: General rules - Supplementary rules for stainless steels. Brussels: CEN 2005.

### Literature

- 4 *Schaumann, P.*: Zur Berechnung stählerner Bauteile und Rahmentragwerke unter Brandbeanspruchung. Ruhr-Universität Bochum: Technisch-wissenschaftliche Mitteilungen 1984 (in German).
- 5 *Kaitila, O.*: Numerical thermal analysis of Kenno Tech wall and floor structures, VTT 29.09.2005
- 6 *VTT*: Stainless steel in fire (SSIF), contract: RFS-CR-04048; WP1 Fire resistant structures and products; Appendix A of mid term report for issue to the RFCS; 1<sup>st</sup> July 2004 to 31<sup>st</sup> December 2005; Document RT1099, version 01 07.03.2006
- 7 *Gardner, L., Ng, K. T.*: Temperature development in structural stainless steel sections exposed to fire. Fire Safety Journal 41 (2006), p. 185–203.
- 8 *Sedlacek, G., Heinemeyer, C.*: Brandsicherheit durch Stahlsortenwahl. Stahlbau 73 (2004), p. 908–915. (in German)
- 9 *Ellobody, E., Young, B.*: Structural performance of cold-formed high strength stainless steel columns. Journal of Constructional Steel Research 61 (2005), p. 1631–1649.
- 10 *Lindner, J., Rusch, A.*: Stützen mit dünnwandigen Querschnittsteilen. Berlin: Technische Universität Berlin 2000. (in German)

### Reports

- 11 *Schaumann, P., Heise, A., Kettner, F.*: Stainless Steel in Fire, WP 1 Fire Resistant Structures and Products, WP 1.5. Numerical Studies - Results “Kenno Tech floor”, Leibniz University Hannover 19.09.2005
- 12 *Schaumann, P., Kettner, F.*: Stainless Steel in Fire, WP 1 Fire Resistant Structures and Products, WP 1.5. Numerical Studies - Results “Kenno Tech floor”, 2<sup>nd</sup> report, Leibniz University Hannover 22.02.2006
- 13 *Schaumann, P., Bahr, O., Kettner, F.*: Stainless Steel in Fire, WP 1 Fire Resistant Structures and Products, WP 1.5. Numerical Studies, 3<sup>rd</sup> report, Leibniz University Hannover 06.10.2006